HHS Public Access

Author manuscript

*Biomaterials*. Author manuscript; available in PMC 2020 September 01.

Published in final edited form as:

*Biomaterials*. 2019 September ; 215: 119177. doi:10.1016/j.biomaterials.2019.04.022.

# Tunable Hydrogels for Controlling Phenotypic Cancer Cell States to Model Breast Cancer Dormancy and Reactivation

**Shantanu Pradhan** and **John H. Slater***

Department of Biomedical Engineering, University of Delaware 150 Academy Street, 161 Colburn Lab, Newark, DE 19716, USA

## Abstract

During metastasis, disseminated tumor cells (DTCs) from the primary tumor infiltrate secondary organs and reside there for varying lengths of time prior to forming new tumors. The time delay between infiltration and active proliferation, known as dormancy, mediates the length of the latency period. DTCs may undergo one of four fates post-infiltration: death, cellular dormancy, dormant micrometastasis, or invasive growth which, is in part, mediated by extracellular matrix (ECM) properties. Recapitulation of these cell states using engineered hydrogels could facilitate the systematic and controlled investigation of the mechanisms by which ECM properties influence DTC fate. Toward this goal, we implemented a set of sixteen hydrogels with systematic variations in chemical (ligand (RGDS) density and enzymatic degradability) and mechanical (elasticity, swelling, mesh size) properties to investigate their influence on the fate of encapsulated metastatic breast cancer cells, MDA-MB-231. Cell viability, apoptosis, proliferation, metabolic activity, and morphological measurements were acquired at five-day intervals over fifteen days in culture. Analysis of the phenotypic metrics indicated the presence of four different cell states that were classified as: (1) high growth, (2) moderate growth, (3) single cell, restricted survival, dormancy, or (4) balanced dormancy. Correlating hydrogel properties with the resultant cancer cell state indicated that ligand (RGDS) density and enzymatic degradability likely had the most influence on cell fate. Furthermore, we demonstrate the ability to reactivate cells from the single cell, dormant state to the high growth state through a dynamic increase in ligand (RGDS) density after forty days in culture. This tunable engineered hydrogel platform offers insight into matrix properties regulating tumor dormancy, and the dormancy-proliferation switch, and may provide future translational benefits toward development of anti-dormancy therapeutic strategies.

### Keywords

Cancer; Dormancy; Metastasis; Relapse; Hydrogel; Tissue Engineering

*Corresponding author. jhslater@udel.edu.

Data Availability

The authors declare that all the relevant data supporting the findings of this study are available within the paper and its supplementary information, and from the corresponding authors upon reasonable request.

## 1. Introduction

Metastasis is a leading cause of cancer-associated mortality worldwide, with a dismal 5-year survival rate of only 26% for metastatic breast cancer patients in the United States [1-3]. Despite recent advances in the detection, diagnosis, and treatment of primary tumors, treatment of metastatic disease remains challenging. One of the major roadblocks toward prevention and treatment of metastasis is a poor understanding of the mechanisms underlying metastatic relapse as well as the factors that mediate latency that often occurs prior to relapse [4-7]. Cancer latency can occur in two general environments, near the primary tumor site and in secondary organs. Cells near the primary tumor that survive treatment can reside in a dormant state before becoming reactivated; which is often termed residual disease. Similarly, disseminated tumor cells (DTCs) that have infiltrated secondary organs can also acquire a dormant state before actively forming new tumors. The latency period for cells in both environments can vary from a few months to a few decades depending on multiple factors including molecular subtype of the primary tumor, microenvironmental regulation, systemic inflammation, and patient lifestyle amongst others [5,6,8-10].

Post infiltration of secondary organs, DTCs can undergo one of four fates: death via apoptosis or autophagy, single cell dormancy or dormant microcluster formation via environmental regulation, or overt growth characterized by aggressive progression. [4]. Recent evidence indicates that many types of DTCs, including those originating from breast tumors, can adopt different dormancy states including cellular dormancy characterized by the presence of solitary, quiescent cells and tumor mass dormancy characterized by small cell clusters that maintain overall tumoral homeostasis through a delicate balance between proliferation and death (dormant micrometastasis) [11,12]. The persistence of DTCs as solitary, dormant cells or dormant cell clusters is, in part, mediated by the stromal microenvironment. This complex milieu consists of signals originating from direct interactions with, and/or paracrine signaling from, stromal cells, endothelial cells, and immune cells as well as chemical and physical regulation from the extracellular matrix (ECM) [13-16]. Identifying mechanisms that mediate dormancy may provide an opportunity to preemptively target dormant tumor populations, delay metastatic relapse, and ultimately prolong patient survival.

The role of the ECM in regulating tumor dormancy and metastatic relapse has gained increasing attention in recent years. ECM-induced dormancy has been achieved via encapsulation of cancer cells in a multitude of both natural and synthetic biomaterials including collagen, agarose, poly(ethylene glycol) (PEG)-based blends, and interpenetrating networks (IPNs) of different materials [4,17]. Tuning matrix properties including stiffness and degradability to mediate cell-matrix interactions and to physically entrap cancer cells have been employed for dormancy-induction in three-dimensional (3D) *in vitro* models [18-21]. However, elucidating the individual contribution of these matrix properties toward dormancy induction and maintenance is necessary to gain deeper insight into mechanisms that mediate dormancy. Additionally, understanding how specific ECM properties regulate DTC fate with respect to inducing death, single cell dormancy, tumor mass dormancy, or

invasive growth could potentially aid development of new therapeutic strategies targeted toward the ECM [22-25].

Another important aspect concerning metastatic disease is the role of the ECM in regulating the dormancy-proliferation switch and escape of DTCs from the dormancy program toward unregulated growth. This phenomenon has been modeled *in vitro* via modulation of matrix properties (e.g. partial or complete enzymatic digestion of 3D matrix) [20], promotion of integrin engagement of dormant tumor cells with the surrounding matrix [26], and the addition of paracrine factors including pro-inflammatory cytokines and angiogenic growth factors to mediate cell cycle progression [27,28]. However, there is a lack of *in vitro* models that permit modulation of ECM properties in a dynamic, temporal manner over extended time periods to facilitate the investigation of the dormancy-proliferation switch of DTCs.

To investigate the influences of ECM biochemical (ligand (RGDS) density and degradability) and physical properties (stiffness and mesh size) on breast cancer cell fate, we developed a set of PEG-based hydrogels containing systematic variations in ligand (RGDS) density and crosslink density and implemented them to quantify the temporal response of encapsulated metastatic breast cancer cells with a focus on tumor dormancy. We employed simple hydrogel formulations composed of a base PEG-macromer containing the enzymatically degradable peptide sequence, GGGPQGIWGQGK, with varying concentrations of the integrin ligating peptide, RGDS (0-10 mM), and the non-degradable, co-monomer N-vinyl pyrrolidinone (NVP) (0-18.7 mM) resulting in 16 different hydrogel formulations. Varying the concentration of NVP allowed for controlled modulation of matrix adhesivity (RGDS conjugation efficiency), bulk stiffness, degradability, and mesh size. The influence of hydrogel properties on the behavior of encapsulated metastatic breast cancer cells with respect to viability, apoptotic death, proliferation, metabolic activity, invasiveness, and cluster formation was quantified over 15 days in culture. Using these metrics, we classified the resultant cancer cell phenotype as a function of hydrogel properties and demonstrated that hydrogels can be tuned to achieve four distinct phenotypic states. These states were classified as: (1) a high growth state characterized by increased proliferation and metabolism, minimal cell death, and a significant increase in cell density and the propensity to form invasive clusters, (2) a moderate growth state characterized by slightly lower proliferation, metabolic activity, and invasiveness compared to the high growth state, (3) a single cell, restricted survival, dormant state where a majority of the cells underwent apoptosis while the surviving cells remained solitary, quiescent and non-invasive with very low proliferation, and (4) a balanced dormancy state characterized by temporal consistency in cell viability, cell density, and metabolism, and a close balance between proliferation and death.

The individual contributions of hydrogel physical and biochemical properties toward induction of cancer cells into specific states is important for mechanistic investigations of ECM-induced dormancy. Despite increasing crosslink density with addition of NVP, differences in hydrogel bulk stiffness in the presence of encapsulated cells were fairly attenuated, and differences in mesh size of the hydrogel matrices were of significantly lower magnitude than the size of encapsulated cells. By deductive inference, matrix degradability and ligand (RGDS) density were postulated to be the major regulators of cancer cell fate in

this study. Overall, physical confinement of cancer cells via modulated matrix adhesivity and degradability helped maintain cancer cells in a dormant state in engineered *in vitro* microenvironments. Furthermore, we demonstrate the ability to phenotypically switch cancer cells from the single cell, restricted survival, dormant state to the high growth state via a dynamic increase in ligand (RGDS) density through 75 days in culture; recapitulative of metastatic relapse. This biomaterial-based regulation of cancer cell phenotype facilitates long-term investigation of ECM-regulated changes in cell phenotype and may be useful for investigating dormancy-associated mechanisms, metastatic relapse, and potentially aid in development of future therapeutic approaches to delay or prevent metastases.

## 2. Materials and Methods

### 2.1 Cell Culture

The triple negative, metastatic breast cancer line, MDA-MB-231, was purchased from American Type Culture Collection (ATCC) and cultured in Dulbecco's Modified Eagle Medium (DMEM: Thermo Fisher) supplemented with 10% (v/v) fetal bovine serum (FBS: Thermo Fisher) and 1% (v/v) penicillin-streptomycin (Lonza). All cells were cultured in fibronectin coated (10 μg/mL) T25 flasks at 37°C and 5% $CO_2$ and grown to 80% confluency before passaging. Prior to encapsulation in hydrogels, cells were serum starved via culture in serum free DMEM for 48 hours. Passages 35-40 were used for all studies.

### 2.2 PEG Macromer Synthesis and Characterization

Acrylate-PEG-SVA (MW: 3400 Da, Laysan Bio), the proteolytically degradable peptide sequence GGGPQG↓IWGQGK (PQ, MW: 1141.24 Da, ↓ denotes cleavage site) and the integrin-ligating peptide sequence RGDS (MW: 433.42 Da) (American Peptide) were purchased. Acrylate-PEG-SVA was reacted with the PQ peptide at a 2.1:1 molar ratio (PEG:peptide) in dimethyl sulfoxide (DMSO) with N,N-diisopropylethylamine (DIPEA) at a 4:1 molar ratio (DIPEA:PQ) at room temperature for 48 hours to form the PEGylated, diacrylated, PEG-PQ-PEG (PEG-PQ) macromer (Fig. 1A). Similarly, acrylate-PEG-SVA was reacted with the RGDS peptide at a 1.1:1 molar ratio (PEG:peptide) in DMSO with DIPEA at a molar ratio of 2:1 (DIPEA:RGDS) to form the PEGylated, monoacrylated PEG-RGDS macromer (Fig. 1B). A fluorophore analog, PEG-RGDS-Alexa Fluor 488 (PEG-RGDS-488) was synthesized in a similar way as PEG-RGDS, with Alexa Fluor® 488 succinimidyl ester (Thermo Fisher, dissolved in DMSO) being added to the reaction mixture, at a 1:1 molar ratio (fluorophore:peptide), of acrylate-PEG-SVA and RGDS after 24 hours of reaction time. In all cases, reacted products were dialyzed against deionized (DI) water for 24 hours with 4 water changes (MWCO 3500, Regenerated Cellulose, Spectrum Laboratories). Dialyzed products were frozen, lyophilized, and stored at −80°C under argon. PEG-peptide conjugation was verified by gel permeation chromatography (GPC, Waters, aqueous phase).

### 2.3 Hydrogel Photopolymerization and Cell Encapsulation

PEG-PQ (MW: 7900 Da) was reconstituted in phosphate-buffered saline (PBS) to a final concentration of 5% w/v (6.3 mM). PEG-RGDS (MW: 3800 Da) was reconstituted in PBS to final concentrations of 0, 1, 5 and 10 mM. N-vinyl pyrrolidinone (NVP) was mixed with

the PEG-PQ and PEG-RGDS precursor solutions to final concentrations of 0.0, 0.5, 1.0 and 2.0 μL/mL (0.0, 4.7, 9.4, and 18.7 mM) with the UV-sensitive photocrosslinker, lithium phenyl-2,4,6-trimethylbenzoylphosphinate (LAP) at a final concentration of 10 mM (Fig. 1C). 500 μm thick poly(dimethyl siloxane) (PDMS) spacers were fabricated using established protocols and 3 mm diameter holes were punched to form molds. For hydrogel characterization studies, 3 μL of polymer precursor solution was pipetted into the molds on a glass slide followed by exposure to UV light (Blak-Ray flood UV lamp, wavelength: 365 nM, intensity: 10 mW/cm$^2$) for 1 minute to form photocrosslinked hydrogels. Hydrogels were transferred to well plates and incubated in PBS at room temperature overnight to ensure removal of unconjugated moieties before use in the various assays described below.

For cell studies, MDA-MB-231s were trypsinized, counted, and re-suspended in prepolymer solution at $10\times10^6$ cells/mL. A strip of Parafilm was stretched on a glass slide to create a hydrophobic surface and 3 μL of the cell-containing polymer precursor solution was pipetted in droplets on the Parafilm surface (Fig. 1C). After UV exposure for 1 minute, photocrosslinked, cell-laden hydrogels were transferred to well plates and cultured in media for at least 15 days or longer, depending on the assay being performed. Cells in hydrogels were imaged under phase contrast every 5 days using an inverted Zeiss AxioObserver Z1 microscope.

### 2.4 Characterization of PEG-RGDS Incorporation

The final concentration of photocoupled PEG-RGDS in acellular PEG-PQ hydrogels as a function of PEG-RGDS (0, 1, 5, and 10 mM) and NVP (0.0, 4.7, 9.4, 18.7 mM) concentrations in the prepolymer solution was quantified via fluorescence imaging and analysis. PEG-RGDS-488 was added to the prepolymer solution at a concentration of 0.5 mM. The concentrations of PEG-RGDS were adjusted to 0.5. 4.5, and 9.5 mM to ensure the total concentrations of PEG-RGDS moieties were equal to 1, 5, and 10 mM respectively. As a control, prepolymer solution containing 0 mM PEG-RGDS-488 was used to quantify the background fluorescence intensity. Imaging was performed using a Zeiss AxioObserver Z1 inverted fluorescent microscope equipped with a Zeiss AxioCam MRm camera. Images were acquired 200 μm from the bottom of the hydrogel to ensure imaging at the same z-location in all hydrogels to account for swelling. A GFP filter cube (excitation: 450-490 nm, emission: 500-550 nm) was used with an excitation intensity of 20 mW/cm$^2$ and acquisition time of 100 ms. The prepolymer solutions were pipetted into PDMS molds and imaged immediately to acquire an unbleached fluorescent baseline image. After 1 minute UV exposure, the hydrogels were imaged again under the same settings and the pre-crosslinked and post-crosslinked fluorescence intensities were analyzed using FIJI software (NIH, Version 1.52h) to obtain the percent reduction in fluorescence due to photobleaching. The bleached hydrogels were rinsed in PBS overnight to remove unconjugated PEG-RGDS and PEG-RGDS-488. Fluorescent images of the rinsed hydrogels were acquired using the same settings and the relative intensities were used to measure the conjugation efficiencies. A replicate of 4 hydrogels were measured for each condition.

The following assumptions were made to quantify the conjugation efficiency using this approach:

1. PEG-RGDS and PEG-RGDS-488 have the same incorporation efficiency.
2. The molecular weights of PEG-RGDS and PEG-RGDS-488 are similar (based on molar ratios used during synthesis).
3. Overnight rinsing ensures complete removal of unconjugated moieties.

The following equations were used to quantify the concentration of conjugated PEG-RGDS in the hydrogels:

$$\text{Relative bleaching (B)} = \frac{I_1}{I_0} \quad (1)$$

where $I_0$ is the fluorescence intensity prior to crosslinking and $I_1$ is the fluorescence intensity immediately after crosslinking which accounts for bleaching.

$$\text{Relative conjugation (C)} = \frac{I_2}{I_1} \quad (2)$$

where $I_2$ is the fluorescence intensity after rinsing and removal of unconjugated moieties.

$$\text{Conjugated PEG-RGDS concentration ([RGDS])} = C \times R \quad (3)$$

Where R is the initial PEG-RGDS concentration in the prepolymer solution (R = 1, 5 or 10 mM PEG-RGDS).

## 2.5 Mechanical Characterization of Hydrogels

PEG-PQ hydrogels were polymerized by pipetting 15 μL of prepolymer solution into 3 mm diameter, 1 mm tall cylindrical PDMS molds followed by photocrosslinking as described in Section 2.3. Hydrogels were either acellular or laden with MDA-MB-231 cells ($10\times10^6$ cells/mL) for 1 or 15 days prior to testing. Cell-laden hydrogels contained 1 mM PEG-RGDS in the prepolymer solution which was assumed to have minimal effect on the compressive modulus of the hydrogel compared to the acellular hydrogels with 0 mM PEG-RGDS. Samples were loaded onto a Universal Testing System 3340 Series (Instron) using platens for unconfined compression testing in the presence of warm PBS. Samples were compressed using a 10 N load cell at 2 μm/s for 100 seconds with an initial load of 0.02 N to ensure uniform contact. The slope of a linear fit of the stress versus strain curve (within the first 20% of the strain compression) was calculated as the compressive modulus. A replicate of 3 hydrogels was used for each condition.

## 2.6 Swelling Ratio

PEG-PQ hydrogels with varying NVP concentrations (0.0, 4.7, 9.4, 18.7 mM) were photopolymerized and allowed to swell to equilibrium in PBS overnight at 4°C. Swollen

hydrogels were weighed in a carefully tared weighing balance and allowed to dry in ambient air for 6 hours. Dried hydrogels were reweighed and the swelling ratio calculated as follows:

$$\text{Swelling ratio} = \frac{\text{Swollen Weight} - \text{Dry Weight}}{\text{Dry Weight}} \quad (4)$$

A replicate of 4 hydrogels was used for each condition.

## 2.7 Degradation Analysis

PEG-PQ hydrogels with varying NVP concentrations (0.0, 4.7, 9.4, 18.7 mM) containing 1 mM methacryloxyethyl thiocarbamoyl rhodamine B (Polysciences) were photopolymerized and allowed to swell in PBS overnight. Collagenase IV (Worthington, 260 U/mg) was prepared in PBS at 100 μg/mL, warmed to 37°C and added to the swollen hydrogels. Hydrogels were incubated at 37°C and imaged at 15-minute intervals over 3 hours using a Zeiss AxioObserver Z1 inverted fluorescent microscope equipped with a Zeiss AxioCam MRm camera. A rhodamine filter cube (excitation: 538-562 nm, emission: 570-640 nm) was used with an excitation intensity of 27 mW/cm$^2$ and acquisition time of 100 ms. The decrease in fluorescence intensity over time during degradation was measured using FIJI software to determine relative degradation. Hydrogels with 0.0 mM NVP incubated in PBS without collagenase were used as a control. This control was included as a reference to correct for any photobleaching of the fluorophore that might occur during time-lapse image acquisition. A replicate of 3 hydrogels was used for each condition.

## 2.8 Characterization of Hydrogel Mesh Size

PEG-PQ hydrogels with varying NVP concentrations (0.0, 4.7, 9.4, 18.7 mM) were photopolymerized and allowed to swell in DI water overnight. 3 kDa and 150 kDa fluorescein isothiocyanate (FITC)-labeled dextran (Thermo Fisher) were dissolved in DI water at 1 mg/mL. Swollen hydrogels were transferred to FITC-dextran solutions and allowed to incubate for 48 hours at 4°C to reach equilibrium. FITC-dextranfilled hydrogels were transferred to fresh well plates, excess solution blotted off, and DI water added to each sample to measure diffusion of FITC-dextran out of the hydrogels into the surrounding water. Samples of the DI water were collected every 15 minutes for 4 hours and the FITC-dextran intensity was measured using a plate reader (Biotek Synergy, Excitation: 490 nm, Emission: 525 nm) until no change in fluorescence intensity was observed. An equal volume of DI water was added at each collection step. Fluorescence intensity values were normalized to the total intensity of released FITC-dextran over the experimental time course. The cumulative mass of FITC-dextran released was analyzed from the measured fluorescence intensities and used to calculate the diffusion coefficient of FITC-dextran according to the equation below [21,29]:

$$\frac{M_t}{M_\infty} = 1 - \frac{8}{\pi^2}\exp\left[\frac{-D\pi^2 t}{4\delta^2}\right] \quad (5)$$

where $M_t$ is the mass of released FITC-dextran at time t, $M_\infty$ is the cumulative mass of FITC-dextran, $M_t/M_\infty$ is the fractional mass of FITC-dextran released, D is the effective diffusion coefficient, and 2δ is the hydrogel thickness (500 μm).

The theoretical mesh size of the hydrogels was estimated using the hindered solute diffusion in solventfilled-pores model based on the following equation:

$$\frac{D}{D_0} = (1-\lambda^2)(1-2.1044\lambda+2.089\lambda^3-0.948\lambda^5) \quad (6)$$

where D is the diffusion coefficient of 150 kDa FITC-dextran in hydrogels, $D_0$ is the diffusion coefficient of 150 kDa FITC-dextran calculated from the Stokes–Einstein's equation ($2.09\times10^{-7}$ $cm^2/s$), and λ is a characteristic ratio of FITC-dextran hydrodynamic diameter to average pore diameter of the hydrogel matrix. The Stokes' radii and hydrodynamic diameter of 150 kDa dextran was estimated to be 8.5 nm and 17 nm respectively, as provided by the manufacturer. A replicate of 4 hydrogels per condition were analyzed.

### 2.9 Quantification of Cell Viability

Cell-laden hydrogels at days 0 (6 hours post encapsulation), 5, 10, and 15 were rinsed twice in PBS for 15 minutes to remove excess media. The rinsed hydrogels were labeled using a Live/Dead® cell viability kit (Invitrogen) in PBS for 30 minutes according to manufacturer's instructions. Labeled hydrogels were rinsed with PBS, transferred onto coverslips and imaged using structured illumination on a Zeiss AxioObserver Z1 inverted fluorescent microscope equipped with a Zeiss Apotome imaging system. Fluorescent z-stacks (z-height: 150 μm, step size: 3 μm) were acquired and analyzed using FIJI software. The number of live and dead cells were manually counted in each z-stack to quantify cell viability and to determine the viable cell density. A minimum of 6 z-stacks from 3 independent hydrogels were quantified for each time point and each hydrogel condition.

### 2.10 Quantification of Early Apoptosis

Cell-laden hydrogels at days 0 (6 hours post encapsulation), 5, 10, and 15 were rinsed twice in 1X HEPES-buffered saline (HBS) supplemented with 2.5 mM $CaCl_2$. Rinsed hydrogels were incubated in a solution containing CF568 Annexin V (Biotium, 1 μg/mL), an early apoptotic marker, at 37°C for 30 minutes. Cells were counterstained with Hoechst 33342 (10 μg/mL) for nuclear staining. Stained cells were rinsed with HBS twice and imaged using structured illumination. Imaging and image analysis were conducted as described in Section 2.9 and the percentage of cells positive for Annexin V quantified. A minimum of 6 z-stacks from 3 independent hydrogels were quantified for each time point and each hydrogel condition.

### 2.11 Quantification of Proliferation

Cell proliferation was measured via 5-ethynyl-2'-deoxyuridine (EdU) incorporation using the Click-It® EdU Imaging Kit (Invitrogen) following the manufacturer's instructions.

Briefly, cell-laden hydrogels were incubated with media containing 10 μM EdU for 24 hours, after which they were rinsed twice with PBS, and fixed with 4% paraformaldehyde at room temperature for 30 minutes. The cells were permeabilized with PBS-T (PBS + 0.2% (w/v) bovine serum albumin + 0.1% (v/v) Triton-X) for 15 minutes and blocked with blocking buffer (PBS + 3% fetal bovine serum) for 30 minutes. Cells were labeled with Alexa Fluor 555 azide (proliferating nuclei) and counter-stained with Hoechst 33342 (all nuclei) and imaged using structured illumination. Imaging and image analysis were conducted as described in Section 2.9. The percentage of nuclei positive for Alexa Fluor 555 was quantified. A minimum of 6 z-stacks from 3 independent hydrogels were quantified for each time point and each hydrogel condition.

### 2.12 Quantification of Metabolic Activity

Metabolic activity of cells encapsulated in hydrogels was assessed using the Alamar Blue assay (Thermo Fisher). Briefly, cells encapsulated in hydrogels were cultured in phenol red-free media. On days 0 (6 hours post encapsulation), 5, 10, and 15, hydrogels were rinsed twice with PBS and incubated in a working solution of Alamar Blue (10 μL of 10X stock + 100 μL phenol red-free media) at 37°C for 4 hours. Resazurin in the working solution was converted to resorufin, the hydrogels were collected, transferred into fresh well plates with phenol red-free media, and the fluorescence intensity of the hydrogels was measured using a plate reader (Biotek Synergy, Excitation: 550 nm, Emission: 600 nm) to assess relative metabolic activity. Wells with phenol red-free media only were used as background controls. All values were normalized to day 0 values for each hydrogel condition. A minimum of 6 independent hydrogels were quantified for each time point and each hydrogel condition.

### 2.13 Quantification of Cell and Cell Cluster Properties

Cell-laden hydrogels were cultured for 15 days, after which they were rinsed twice in PBS and fixed in 4% paraformaldehyde for 30 minutes at room temperature. The cells were permeabilized with PBS-T for 20 minutes, blocked with blocking buffer for 30 minutes, incubated with Alexa Fluor 568 phalloidin (Invitrogen) (25 μL/mL) for 1 hour (for F-actin staining) and counterstained with Hoechst 33342 (10 μL/mL) (for nuclear staining) for 30 minutes. The cell-laden hydrogels were rinsed twice in PBS and imaged via confocal microscopy (Zeiss LSM 710) to obtain 3D z-stacks (excitation: 405 nm, 561 nm; emission: 483 nm, 600 nm). 5 z-stacks (z-height: ~150 μm, step size: 3 μm) were obtained for each hydrogel condition and analyzed using FIJI software. Individual cells and cell clusters were manually traced and the percentage of single cells vs. clustered cells, rounded cells vs. invasive cells, non-invasive vs. invasive clusters, and single cell and cluster density were quantified for each hydrogel condition. Invasive cells/cell clusters were identified as those with a roundness value less than 0.80. In addition, for cell clusters, the projected area, Feret diameter, aspect ratio, circularity, and roundness were also quantified.

### 2.14 Classification of Cell States and Phenotypic Dormancy Metrics

To categorize cancer cell states as a function of hydrogel properties, specific phenotypic metrics (normalized viable cell density, normalized metabolic activity, new live and dead cell densities post encapsulation, and cluster features) measured on day 15 for each of the 16 hydrogel formulations were comparatively analyzed. A scatter plot of normalized viable cell

density against normalized metabolic activity, both values normalized to day 0 values, was generated. Three distinct hydrogel clusters were observed. The cluster with high values for both metrics was assigned as a ‘high growth state’ and the cluster with low values for both metrics was assigned as a ‘single cell, restricted survival, dormancy state’. For hydrogels in the remaining cluster, the new live cell density post encapsulation (cells/$mm^3$) was plotted against the new dead cell density post encapsulation (cells/$mm^3$). The live and dead cell density in each hydrogel formulation on days 5, 10 and 15 was measured from viability and cell density measurements and the cumulative new live and new dead cell densities post encapsulation were calculated. The average standard deviation of measurements from all hydrogels was used to determine the uncertainty in the measurements; shown as deviation from the line with slope of 1. Hydrogels with a higher new live cell density compared to new dead cell density (falling beyond the bounds of the slope) were classified as a ‘moderate growth state’ while those with balanced new live and dead cell densities (falling within the indicated bounds) were classified in a ‘balanced survival, dormancy state’ and subjected to further analysis. A scatter plot of the percentage of clustered cells versus the cluster density was generated and two clusters were observed, one inducing ‘low density clusters’ and the other inducing ‘high density clusters’. Further, all measured metrics were normalized to the highest and lowest value measured for each metric on day 15. For each metric, a value of 0.0 and 1.0 corresponded to the lowest and highest measured value among all 16 hydrogel formulations respectively. The normalized values were displayed as a heatmap and the 16 hydrogel formulations were categorically grouped to elucidate differences and commonalities among each phenotypic state.

### 2.15 Reactivation of Dormant Tumor Cells

MDA-MB-231 cells were encapsulated in 5% (w/v) PEG-PQ hydrogels with 0 mM NVP and 0 mM PEG-RGDS. Live/Dead staining and EdU uptake assays were conducted every 15 days. On day 40, 10 mM PEG-RGDS in PBS containing 10 mM LAP photoinitiator was prepared. Hydrogels were removed from media, rinsed twice in PBS for 15 minutes and incubated in the PEG-RGDS solution for 1 hour at 37°C to allow diffusion of PEG-RGDS into the hydrogel matrix. After 1 hour, hydrogels were removed, exposed to UV light for 1 minute to photocouple PEG-RGDS to the PEG-PQ matrix, and cultured for another 35 days. Cell viability, viable cell density, and proliferation were quantified as described above 5, 15, and 35 days post PEG-RGDS coupling. A minimum of 6 z-stacks from 3 independent hydrogels were quantified for each time point and each hydrogel condition.

### 2.16 Statistical Analysis

All statistical analyses were conducted using Minitab 18 Statistical Software (Minitab Inc.). Normality of distribution and equality in variance among groups were evaluated. Assuming equal sample size of compared groups, one-way analysis of variance (ANOVA) with Tukey's family error rate of 5% was used to evaluate statistical significance between multiple groups. In the case of unequal variance, the Games-Howell post-hoc test was employed following the ANOVA analysis. Unless otherwise indicated, $p < 0.05$ was considered statistically significant.

# 3. Results

## 3.1 The Influence of NVP Concentration on PEG-PQ Hydrogel Properties

A set of complementary hydrogels containing systematic variations in ligand and crosslink density were generated using three components: PEG-PQ, PEG-RGDS, and NVP. The PEG-PQ macromer was held constant at 5% (w/v) while the concentration of the integrin-ligating ligand, PEG-RGDS (0-10 mM), and the non-degradable co-monomer, NVP (0-18.7 mM), were varied (Fig. 1). The PEG-PQ backbone macromer allows cell-mediated degradation through matrix-metalloproteases (MMPs), including MMPs-2 and -9 [30]. The PEG-RGDS moiety allows integrin-mediated cell adhesion and tuning its concentration provides control over matrix adhesivity. The NVP moiety, on account of its acrylate side groups, provides additional crosslinks [31,32]. The concentration of PEG-RGDS in the prepolymer solution was either 0, 1, 5, or 10 mM. The concentration of NVP was 0.0, 4.7, 9.4, or 18.7 mM, which resulted in an increasing NVP/acrylate ratio of 0.00, 0.37, 0.74, and 1.48 and an increasing theoretical crosslink density of 0.0126, 0.0127, 0.0220, and 0.0313 mol/L in the hydrogels respectively.

To assess the influence of NVP on hydrogel properties, the following metrics were quantified: (1) PEG-RGDS concentration post crosslinking and rinsing, (2) compressive moduli with and without encapsulated cells, (3) swelling, (4) degradability, and (5) diffusion of dextran which was used to calculate (6) the theoretical mesh size of the hydrogels.

**3.1.1 RGDS Incorporation—**The presence of NVP significantly enhanced incorporation of PEG-RGDS into the hydrogels. In the absence of NVP (0.0 mM), the average conjugation efficiency of PEG-RGDS was 20.4 ± 1.1% for all PEG-RGDS concentrations, but in the presence of NVP (4.7-18.7 mM) conjugation efficiency increased significantly to 82.3 ± 2.5%. The increased conjugation efficiency is attributed to the presence of additional acrylates provided by the NVP and the increased NVP/acrylate ratio in the hydrogels. Hydrogels with 0 mM NVP contained final PEG-RGDS concentrations of 0.2, 1.1, and 1.9 mM while those with 4.7-18.7 mM NVP contained 0.8, 4.2, and 8.2 mM for 1, 5, and 10 mM PEG-RGDS in the prepolymer solutions respectively (Fig. 2A).

**3.1.2 Compressive Moduli—**The presence of NVP also increased the bulk compressive moduli of acellular hydrogels in a concentration-dependent manner, due to increased crosslinking of the PEG-PQ macromer (Fig. 2B). Compressive moduli of acellular hydrogels were 5.8, 15.1, 18.1, and 27.2 kPa for corresponding NVP concentrations of 0.0, 4.7, 9.4, and 18.7 mM. However, the observed increase in hydrogel elasticity was attenuated in the presence of encapsulated cells (as measured on day 0). Cellular hydrogels crosslinked with 4.7, 9.4, and 18.7 mM NVP had reduced compressive moduli of 9.7, 12.3, and 14.0 kPa respectively. Potential causes of the measured decrease in elasticity with encapsulated cells may arise from multiple factors including substitution of hydrogel volume with cell volume and the inherent lower elasticity of cells (<1 kPa) compared to the acellular hydrogel matrix. For hydrogels with 0 mM NVP, cellular hydrogels appeared stiffer than acellular hydrogels (though not significantly different), possibly due to limitations in detection sensitivity of the compression testing system in the range measured. The compressive moduli of cell-laden

hydrogels on day 15 were significantly lower than corresponding values on day 0: 3.0, 3.6, 6.3, and 6.9 kPa for NVP concentrations of 0.0, 4.7, 9.8, and 18.7 mM respectively. This is possibly due to cell-mediated hydrogel degradation over 15 days in culture. Although moduli of cellular hydrogels on days 0 and 15 increased significantly with increasing NVP concentration, the observed difference was not as pronounced as compared to that of acellular hydrogels. These moduli values correspond well with those obtained in previous studies with PEG-PQ hydrogels crosslinked with photopolymerization of Eosin Y in the presence of 16.5 mM NVP (~15-25 kPa) [30,33,34]. The presence of incorporated PEG-RGDS is expected to have minimal effect on the bulk compressive modulus of acellular hydrogels compared to the presence of NVP as previously demonstrated [32].

**3.1.3 Hydrogel Swelling—**The effect of NVP concentration on hydrogel swelling was assessed and it was observed that increased NVP induced a gradual reduction in swelling from 1,725 ± 90% (0 mM NVP) to 1,188 ± 41% (18.7 mM NVP) due to increased crosslink density (Fig. 2C).

**3.1.4 Hydrogel Degradability—**To quantify the influence of adding additional, non-degradable crosslinks via NVP on hydrogel degradability, hydrogels were exposed to collagenase IV and the degradation quantified with time via fluorescence imaging and analysis. Hydrogels with 0 mM NVP underwent complete degradation in 165 minutes (Fig. 2D). However, hydrogels with 4.7, 9.4, and 18.7 mM NVP underwent partial degradation (83, 80, and 65% respectively) over 2 days. The reduction in hydrogel degradability may be attributed to two factors, non-degradability of the NVP co-monomer and reduced accessibility of the PQ peptide sequence in hydrogels with higher crosslink density. To verify whether degradability was hindered by reduced accessibility of degradable moieties to collagenase IV, the diffusion coefficient of collagenase IV was estimated according to equation (5). In this case, $M_t/M_\infty$ is the fractional mass of the degraded hydrogel, and D is the effective diffusion coefficient of collagenase IV. In hydrogels with 0.0, 4.7, 9.4, and 18.7 mM NVP, the effective diffusion coefficients were calculated as $11.28\times10^{-8} \pm 7.41\times10^{-8}$ $cm^2/s$, $3.84\times10^{-8} \pm 1.09\times10^{-8}$ $cm^2/s$, $3.05\times10^{-8} \pm 0.15\times10^{-8}$ $cm^2/s$, and $2.21\times10^{-8} \pm 0.20\times10^{-8}$ $cm^2/s$ respectively. The gradual reduction, but no significant differences, in the effective diffusion coefficients indicates that hindered enzyme transport plays a negligible role in matrix degradability. Considering the high proteolytic concentration of collagenase used for the degradation assay (26 U/mL), it is expected that the rate of hydrogel degradation would be higher than the rate of collagenase diffusion through the hydrogel network. Therefore, reduced hydrogel degradation was primarily mediated by the inherent nondegradability of the NVP co-monomer.

**3.1.5 Diffusion Behavior & Mesh Size—**The effect of NVP concentration on the diffusion of fluorescent dextran was investigated to determine differences in the mesh size of hydrogels. The release of small molecule FITC-dextran of two molecular weights (3 kDa and 150 kDa) from the hydrogel was quantified over 255 minutes to obtain effective diffusion coefficients for the two species. For the 3 kDa FITC-dextran, the effective diffusion coefficients in hydrogels with 0.0-18.7 mM NVP varied from $1.39\times10^{-7} \pm 7.60\times10^{-9}$ $cm^2/s$ to $1.20\times10^{-7} \pm 1.52\times10^{-8}$ $cm^2/s$, with no significant difference between

groups (Fig. 2E). However, in the case of 150 kDa FITC-dextran, the effective diffusion coefficients significantly reduced from $1.01\times10^{-7} \pm 6.55\times10^{-9}$ $cm^2/s$ (0.0 mM NVP) to $6.76\times10^{-8} \pm 1.72\times10^{-8}$ $cm^2/s$ (18.7 mM NVP) (Fig. 2E). These differences in release kinetics can be attributed to differences in molecular weight of the two species. 3 kDa FITC-dextran, owing to its smaller size, may be able to diffuse unhindered through the hydrogels with increased crosslink density, while 150 kDa FITC-dextran, owing to its larger size, may encounter higher diffusive resistance from a more densely crosslinked macromolecular network. These values are in accordance with previous observations of diffusive behavior in PEG-PQ hydrogels measured using protein molecules of molecular weights ranging from 5.7 to 44 kDa, with Stokes radii of 1.3-2.6 nm [33].

To estimate differences in theoretical mesh size due to additional hydrogel crosslinking, the hindered solute diffusion in solvent-filled pores model was employed based on the diffusive behavior of 150 kDa FITC-dextran [21,35]. The estimated theoretical mesh size for hydrogels significantly reduced from 69 ± 5 nm (0.0 mM NVP) to 51 ± 9 nm (18.7 mM NVP), indicating that higher crosslink density of PEG-PQ hydrogels lends increased transport resistance to species of higher molecular weight (Fig. 2F). However, these mesh size values are sufficiently large enough to allow diffusion of nutrients, metabolites and oxygen necessary for cell growth.

### 3.2 Influence of Hydrogel Properties on Cell Viability and Early Apoptosis

To assess the role of hydrogel physical and biochemical properties on encapsulated cell fate, the viability (Fig. 3A-E) and early apoptosis (Fig. 3F-J) of MDA-MB-231 cells was evaluated at 5-day intervals for 15 days. Cell viability on day 0 (6 hours post encapsulation) was 83.9 ± 3.8% across all hydrogel formulations, indicating high viability and low phototoxicity during photopolymerization (Fig. 3B). A steady decrease in cell viability was observed in hydrogels containing 0 mM PEG-RGDS that reached a low of 39.4 ± 4.9% by day 15, likely due to the lack of integrin-ligation to the matrix (Fig. 3C-E). However, viability remained relatively high (82.7 ± 7.1%) in all other hydrogel formulations through day 15. Fluorescent images revealed the presence of large cell clusters with filopodial protrusions, indicative of invasive, aggressive tumor progression in hydrogels with 0 mM NVP and 1-10 mM PEG-RGDS (Fig. 3A). In other formulations (9.4-18.7 mM NVP and 1-10 mM PEG-RGDS), cells predominantly appeared as either single cells or small, rounded clusters, recapitulative of indolent micrometastases [11,36]. Hydrogels with 0 mM PEG-RGDS displayed solitary viable cells distributed amongst a mostly dead cell population. Overall, these results demonstrate that the presence of PEG-RGDS, even at low concentrations, is sufficient to maintain high viability, and that NVP in the range of 4.7-18.7 mM does not significantly influence viability.

In addition to viability, cells undergoing apoptotic death were also quantified by labeling for the early apoptosis marker, annexin V. On day 0 (6 hours post encapsulation), in all hydrogel formulations, cells generally displayed low staining for annexin V (2.6 ± 1.6% of all cells were positive), reconfirming low cytotoxicity during photopolymerization (Fig. 3G). Cells in hydrogels with 0 mM PEG-RGDS displayed a high degree of early apoptosis (55.7 ± 7.7%) on day 15, consistent with the viability data (Fig. 3F-J). However, hydrogels containing

PEG-RGDS (1-10 mM) displayed significantly lower early apoptosis (15.4 ± 4.1%) through day 15, irrespective of NVP concentration. These results reinforce the observation that the presence of PEG-RGDS, even at low concentrations, prevents apoptosis and maintains high viability. Notably, the majority of DTCs that infiltrate secondary organs often undergo apoptosis thereby leading to inefficiency in the hematogenous route of metastasis [4]. Hence, observations in the 0 mM PEG-RGDS hydrogels may correlate well with the native scenario in recapitulating the fate of DTCs in secondary microenvironments.

### 3.3 Influence of Hydrogel Properties on Proliferation, Cell Density and Metabolic Activity

In addition to viability and apoptosis, the fate of encapsulated MDA-MB-231 cells was also monitored through quantification of proliferation, viable cell density, and metabolic activity. Proliferation was estimated indirectly as a measure of cell cycle progression ($G_0/G_1$ transition), via incorporation of EdU within newly synthesized DNA of dividing cell populations. Cells positive for EdU incorporation were classified as proliferative (Fig. 4A). On day 0 (24 hours post encapsulation), the percent of $EdU^+$ cells in all hydrogel formulations was 10.8 ± 1.4%, consistent with that in 2D cultured cells with 48 hours of serum starvation (Fig. 4B). Through day 15, in hydrogels with 0 mM NVP, proliferation increased with increasing PEG-RGDS concentration (up to 47.2 ± 4.1% in 10 mM PEG-RGDS hydrogels on day 15), possibly due to increased cell-matrix adhesion and a high degree of matrix permissiveness (high degradability, larger mesh size) (Fig. 4B-E). However, with increasing NVP concentration (4.7-18.7 mM), proliferation was restricted to lower values (10.0 ± 5.2% on day 15), irrespective of PEG-RGDS concentration. This was possibly due to additional crosslink density (and reduced degradability and mesh size) that physically restricted cancer cells from undergoing division and confined them in a state of cell cycle arrest.

Concomitant with proliferation, the viable cell density, as measured using viability images, also showed dual dependence on PEG-RGDS and NVP concentrations (Fig. 4F-I). On day 0 (6 hours post encapsulation), viable cell density was measured to be 8,612 ± 378 cell/$mm^3$ for all hydrogel formulations (Fig. 4F). Through day 15, in hydrogels with 0 mM PEG-RGDS, viable cell density dropped significantly to 4,209 ± 509 cell/$mm^3$, owing to high levels of apoptosis and low proliferation (Fig. 4I). In hydrogels with 0-4.7 mM NVP and 1-10 mM PEG-RGDS, viable density increased significantly with increasing PEG-RGDS concentration (16,779 ± 4,516 cell/$mm^3$ on day 15), owing to increased proliferation and matrix permissiveness. However, in hydrogels with 9.4-18.7 mM NVP, viable cell density increased moderately (10,699 ± 593 cell/$mm^3$) through day 15, irrespective of RGDS concentration.

In terms of the normalized viable cell density (normalized to day 0 values), quantification at day 15 revealed a 0.5-fold decrease in hydrogels with 0 mM PEG-RGDS (regardless of NVP concentration), a 2.9-fold increase in hydrogels with 0 mM NVP and 10 mM PEG-RGDS, and a 1.2-fold increase in hydrogels with 9.4-18.7 mM NVP and 1-10 mM PEG-RGDS. In general, these observations are in accordance with a close, though not exact, balance between proliferation and apoptotic death, in hydrogels with 9.4-18.7 mM NVP. The results also underscore the role of increased matrix crosslink density, and subsequent decrease in

degradability, in restricting proliferation and maintaining viability to maintain overall tumoral homoeostasis.

The metabolic activity of encapsulated cells in hydrogels with varying PEG-RGDS and NVP concentrations also showed similar trends as proliferation and viable cell density above (Fig. 4J-M). Hydrogels with 0 mM NVP and 1-10 mM PEG-RGDS showed significantly increased metabolic activity through day 15 depending on PEG-RGDS concentration (7.93 ± 4.02-fold increase normalized to day 0), owing to increased proliferation and viable cell density. Hydrogels with 0 mM PEG-RGDS displayed decreased metabolic activity due to significant cell death (0.67 ± 0.12- fold decrease on day 15 normalized to day 0). However, hydrogels with 4.7-18.7 mM NVP showed a moderate increase in metabolic activity when normalized to day 0 values (2.49 ± 0.67-fold increase on day 15 normalized to day 0), in accordance with previous observations of low proliferation and near constant viable cell density.

Further, metabolic activity values were normalized against viable cell density values in each hydrogel formulation, at each time point, to estimate metabolic activity on a per viable cell basis. Cells in hydrogels with 0 mM NVP and 1-10 mM PEG-RGDS displayed a distinct increase in cellular metabolic activity dependent on matrix adhesivity as compared to day 0 values (3.19 ± 0.98-fold increase normalized to day 0). Interestingly, values for other hydrogel formulations did not show a clear trend, indicating that surviving dormant (or low proliferative) cell populations do not undergo a significant change in metabolic activity over the course of 3D culture. Notably, metabolic activity measured here is a combined effect of two cooperative, and competitive, pathways: glycolysis and oxidative phosphorylation. While the relative contribution of each mechanism toward overall cancer cell metabolism in different hydrogel formulations is not known, it would be of interest to probe the dependency of encapsulated cells on either mechanism induced by varying matrix properties.

Overall, proliferation, viable cell density and metabolic activity were observed to be jointly regulated by matrix crosslink density, degradability and matrix adhesivity and modulating these parameters can provide a roadmap toward control of breast cancer cell phenotypic states within engineered hydrogels.

### 3.4 Regulation of 3D Morphology via Tuning of Hydrogel Properties

To assess the influence of hydrogel properties on regulating invasiveness and formation of micrometastatic cell clusters, encapsulated cells were fixed, fluorescently labeled for F-actin, and counterstained with Hoechst (nuclei) on day 15 post encapsulation. The percentage of the cell population existing as single cells or cell clusters was quantified and the density and shape characteristics indicative of invasiveness measured. Hydrogels with 0.0-4.7 mM NVP and 1-10 mM PEG-RGDS showed increasing percentages of cells in clusters (70.6 ± 22.7% of total cells), as invasive single cells (50.0 ± 30.8% of total cells), as invasive cell clusters (66.5 ± 26.8% of total clusters) and a high cluster density (1,348 ± 444 clusters/$mm^3$), with increasing PEG-RGDS concentration (Fig. 5A-F). Additionally, fluorescent images also revealed a high degree of cellular protrusions and elongated colony features (Fig. 5A). These observations are recapitulative of invasive growth dependent on

increasing cell-matrix adhesive interactions. Hydrogels with 0 mM PEG-RGDS contained a high percentage of single cells (89.4 ± 5.1% of total cells), which were rounded and non-invasive (99.3 ± 0.5% of total cells), and a low cluster density (256 ± 156 clusters/$mm^3$) with absence of invasive clusters, likely due to lack of integrin ligation with the matrix. Hydrogels with 9.4-18.7 mM NVP and 1-10 mM PEG-RGDS contained variable percentages of clustered cells (19.0 – 52.6% of total cells) and low percentages of invasive cells (8.4 ± 3.3% of total cells) and invasive cell clusters (16.2 ± 3.9% of total clusters). Interestingly, hydrogels with 9.4 mM NVP, 10 mM PEG-RGDS and those with 18.7 mM NVP, 1-10 mM PEG-RGDS displayed high cluster density (1,370 ± 86 clusters/$mm^3$), simulative of dormant micrometastasis. Notably, rounded, non-invasive, single cells quantified here may include dead cells which may have undergone apoptosis prior to day 15 of morphometric analysis. Hence, while single cell density varied across different hydrogel formulations, this metric is not as predictive of invasiveness or dormancy as compared to cell clusters which resulted only from growth of live cells (Fig. 5F).

Further morphometric analysis of cluster features revealed that hydrogels with 0.0 mM NVP and 1-10 mM PEG-RGDS displayed clusters with high area (2,435 ± 461 $\mu m^2$), diameter (75 ± 10 μm), aspect ratio (1.66 ± 0.06), and low circularity (0.68 ± 0.06) and roundness (0.67 ± 0.02), dependent on PEG-RGDS concentration, all indicative of invasive and aggressive growth. Hydrogels with 0 mM PEG-RGDS displayed clusters with the lowest area (445 ± 85 $\mu m^2$), diameter (28 ± 3 μm) and invasiveness, while other hydrogel formulations displayed intermediate sized clusters (area: 705 ± 233 $\mu m^2$, diameter: 34 ± 6 μm) with low invasiveness. These morphometric observations were also corroborated with phase contrast images which demonstrated the presence of increased large clusters in hydrogels with 0.0 mM NVP and 1-10 mM PEG-RGDS while high numbers of single, rounded cells were observed in hydrogels with 0 mM PEG-RGDS, and intermediate numbers of single cells and clusters in the remaining hydrogel formulations. Overall, these observations are in accordance with previously measured cellular metrics supporting the dual role of matrix crosslink density and matrix adhesivity in regulating cell-matrix interactions and physical confinement of cells toward dormant phenotypes [19,21,37,38].

### 3.5 Phenotypic Classification of Cancer Cell States

The above data indicates that hydrogel properties influence the fate of encapsulated MDA-MB-231 cells. To better elucidate the role of hydrogel properties in dictating cancer cell fate, a phenotypic classification scheme was implemented based on the quantified cell metrics. First, normalized viable cell density was plotted against normalized metabolic activity on day 15, both normalized against day 0 values, for cells in each hydrogel formulation (Fig. 6A). Cells cultured in hydrogels with high values for both metrics were grouped into a ‘high growth state’ and those with low values (<1) for both metrics were grouped into a ‘single cell, restricted survival state’. The remaining hydrogel formulations (Cluster A) were analyzed for a balance between live and dead cell densities post encapsulation (Fig. 6B). The live and dead cell densities for each hydrogel formulation post encapsulation were quantified. The line with slope of 1 represents a perfect balance between the new live cell density and the new dead cell density arising over the course of the 15-day culture period. This balanced growth/death parameter space represents a dormant tumor state where the

population of viable tumor cells remains fairly constant over time. Values above this line represents the parameter space where live cell density increases faster than dead cell density, thereby showing a moderate or slow increase in cell density. Accordingly, hydrogels displaying higher live cell density compared to dead cell density were grouped into a ‘moderate growth state’. The remaining hydrogels (Cluster B) fell within the error band of balanced live and dead cell density (dotted and dashed orange lines) indicating a balance between growth and death and the cells in hydrogels in this cluster were characterized as a ‘balanced dormancy state’. This cluster was further evaluated for cluster features by plotting the percentage of the cell population residing in cell clusters versus the cluster density. The data indicates that all 6 hydrogel formulations have similar percentages of cells residing in cell clusters but that hydrogels with the highest crosslink density had a significantly higher cluster density.

To obtain a comprehensive view of the cell metrics pertaining to each cell state, the quantified cellular metrics were scaled against a phenotype score ranging from 0.0 to 1.0 and visualized using a heatmap (Fig. 6D). The measured cell metrics on day 15 were normalized to the highest (1.0) and lowest values (0.0) for each corresponding metric and were clustered based on the hydrogel classification scheme described above. From the generated heatmap, cells encapsulated in hydrogels containing 0.0 mM NVP and 5-10 mM PEG-RGDS (high growth state) had the highest scores for viability, viable cell density, proliferation, cellular metabolic activity, invasiveness, and the lowest apoptotic cell death and single cell density. Hydrogels with 0 mM PEG-RGDS (single cell, restricted survival, dormancy state) displayed completely contrasting scores for these features, in accordance with previous observations. Hydrogels with 0.0 mM NVP and 1 mM PEG-RGDS and those with 4.7 mM NVP and 1-10 mM PEG-RGDS (moderate growth state) were characterized by high scores for viability but lower scores for other growth/invasion metrics compared to the high growth state thereby indicating that lowering matrix adhesivity or increasing matrix crosslink density significantly reduced the growth and invasive potential. Cells cultured in hydrogels that induced the balanced dormancy state (9.4 mM NVP or 8.7 mM NVP and 1-10 mM PEG-RGDS) displayed lower scores for cell and cluster invasiveness and cluster area compared to the two growth states. These observations underscore the hypothesis that tumor dormancy can be induced by conjointly increasing matrix crosslink density with a non-degradable comonomer and decreasing matrix adhesivity, which results in physical confinement of encapsulated cancer cells and restricted cell-matrix interactions.

Overall, this phenotypic classification scheme facilitated the categorization of hydrogel formulations into groups that support specific cancer cell states, recapitulative of DTCs in the secondary niche post extravasation. Additionally, factors underlying these phenotypic changes were also attributed to specific physical and biochemical properties of the hydrogel formulations. This analysis provides a clear demarcation within the hydrogel property space for directing the fate of model DTCs toward specific states.

### 3.6 Dynamic Switching Between Cancer Cell States

Metastatic recurrence occurs when single dormant tumor cells or dormant microclusters, upon being activated by microenvironmental cues, switch from a dormant state to a growth

state. Some of these cues include altered presentation of ECM proteins, stromal secretions, or integrin ligation with matrix proteins. In this study, the ability to dynamically tune matrix adhesivity (and subsequently cell-matrix interactions) that enables a phenotypic switch from dormancy to growth was demonstrated. Hydrogels with 0.0 mM NVP and 0 mM PEG-RGDS were used for long-term culture of MDA-MB-231 cells to induce a single cell, restricted survival, dormant state that was verified through quantification of viability, viable cell density and proliferation on days 0, 15 and 30 post encapsulation (Fig. 7A-C). In the absence of PEG-RGDS, viability dropped significantly from 85.9 ± 2.9% to 36.2 ± 4.8% over 30 days with a simultaneous decrease in viable cell density from 8,511 ± 774 cells/$mm^3$ to 1,135 ± 203 cells/$mm^3$ and low proliferation at 7.7 ± 2.5 %. The live cells appeared as solitary, single cells interspersed among a majority of dead cells. On day 40, a solution containing 10 mM PEG-RGDS was added to the hydrogels and chemically coupled via photocrosslinking. Post coupling of PEG-RGDS, cell viability and proliferation increased significantly over an additional 35 days in culture to 89.9 ± 4.7% and 61.1 ± 4.8% respectively. The reactivated, previously dormant single cells were able to proliferate and reach a viable cell density similar to day 0 values (8,300 ± 1,895 cells/$mm^3$). Reactivated cells also showed increased spreading, filopodial protrusions, and cluster formation with similar values to those cultured in 0 mM NVP and 10 mM PEG-RGDS hydrogels. While PEG-RGDS coupling is a simple approach to induce reactivation, the results are reminiscent of the dormancy-proliferation switch and invasive regrowth, which may occur in native conditions due to stromal deposition of integrin-ligating proteins. Overall, dynamic modulation of matrix adhesivity enabled the switch from a single cell, restricted survival, dormancy state to a high growth state and recapitulation of the metastatic relapse phenomenon.

## 4. Discussion

Tumor dormancy and the cancer latency period are important considerations toward long-term control and prevention of metastasis. Though modeling of the metastatic cascade using *in vitro* systems has been widely studied, modeling of tumor dormancy and cancer cell quiescence in engineered hydrogels is still in a nascent phase and gaining rapid attention [4,17,24]. In this study, we utilized the systematic tuning of hydrogel adhesivity and crosslink density to mimic potential fates of DTCs in foreign microenvironments of secondary organs post extravasation. Although this is a simplistic approach toward modeling of complex organ-specific microenvironments, specific hydrogel formulations implemented here may recapitulate some aspects of matrix conditions that induce tumor dormancy. Hydrogels lacking adhesive ligands (0 mM PEG-RGDS) mimic when DTCs in secondary organs fail to establish integrin-mediated adhesion required for matrix engagement and survival [39]. Hydrogels with the lowest degradability (18.7 mM NVP) may mimic the situation where DTCs are unable to locally degrade the matrix of the foreign microenvironment. By exploring the adhesivity and crosslink density landscape, we demonstrate that both factors influence breast cancer cell fate and that careful tuning of these hydrogel properties can be implemented to induce a desired response; at least over 15 days in culture. Using NVP as a comonomer in the polymer precursor, the matrix adhesivity, crosslink density, stiffness, and mesh size were altered across different hydrogel

formulations. Differences in bulk compressive moduli of hydrogels, particularly in the presence of cells, were fairly attenuated. Differences in theoretical mesh size between hydrogels was significantly small compared to size of cells. Hence, by deduction, matrix degradability and adhesivity are surmised to have the highest degree of influence over regulation of cancer cell fate but warrant future studies for validation. Furthermore, we demonstrate that a dynamic increase in hydrogel adhesivity results in reactivation of cells from a dormant state to an actively proliferative state.

One of the key considerations toward developing an *in vitro* tumor dormancy model is achieving a delicate balance between cell proliferation and death over extended time periods, thereby sustaining an overall tumoral homeostasis (with constant viability and viable cell density). Toward this end, we have demonstrated the maintenance of MDA-MB-231 cells in states of single cell restricted survival dormancy (death >> proliferation), balanced dormancy (death ≈ proliferation), low growth (death < proliferation) and high growth (death << proliferation) over at least 15 days in culture (Fig. 8). Previous studies on ECM-mediated tumor dormancy demonstrated that physical confinement of cancer cells within dense, non-degradable matrices restricts cells from forming invasive protrusions, limits cell cycle progression and potentially induces apoptotic cell death over 7 days in culture [18,19]. Similarly, we observe that matrix physical and biochemical properties jointly regulate these different states of cancer cells (Fig. 8). When encapsulated in the softest hydrogels with high degradability and high adhesivity, cancer cells are directed toward the high growth state (characterized by high viability, proliferation, metabolic activity, and large sized, high density, invasive clusters). When hydrogel adhesivity is lowered, or crosslink density is slightly raised (with a small increase in stiffness and small reduction in degradability), cancer cells are induced toward a moderate growth state (characterized by high viability, but moderate proliferation, metabolic activity, and moderate-sized, high density, invasive clusters). When hydrogel crosslink density is increased further, cancer cells are restricted to a state of balanced dormancy (characterized by high viability, low proliferation, moderate metabolic activity, and presence of low or high density, non-invasive clusters). Finally, with complete absence of matrix adhesivity (irrespective of crosslink density), cancer cells are directed toward a single cell, restricted survival, dormant state (characterized by low viability, proliferation, metabolic activity, and no cluster formation). In this study, cellular metrics pertaining to dormancy have been quantified over a 15-day culture period. As cancer latency periods tend to span years to decades [9], longer culture periods (~3-4 weeks) would be helpful in simulating and determining: 1) the furthest time point to which these states can be maintained in the respective hydrogel formulations and 2) spontaneous phenotypic switching of cancer cells from one state to another within the same hydrogel formulation.

One limitation of the present acrylate-based crosslinking scheme is that several matrix properties are changed through the introduction of the non-degradable comonomer NVP. Increasing NVP concentration leads to increased crosslink density and in turn, increased compressive moduli and RGDS coupling with simultaneously decreased mesh size and hydrogel degradability. Decoupling the influence of these properties (stiffness, degradability, mesh size, adhesivity) and their independent control is necessary to further elucidate the dominant factor inducing cellular quiescence and dormancy [40,41]. From material characterization studies, it is evident that with addition of NVP, compressive moduli of the

cell-encapsulated PEG-PQ hydrogels increased over a moderate range. The temporal variation in stiffness detected by individual dormant or invasive tumor cells in the immediate vicinity of their surrounding matrix would be of further interest. From the present data, it can be surmised that this range would vary between ~9-27 kPa at the initial time point (when cells are dispersed as single cells and would mostly sense the hydrogel matrix in the immediate vicinity) to ~3-7 kPa at the final time point (when cells form clusters, degrade the local matrix and sense the lower stiffness of adjoining cells).

Similar to stiffness changes, diffusion of small molecule dextran (150 kDa) and mesh size were also observed to vary with NVP concentration. With increasing crosslink density, the effective diffusion coefficient was observed to decrease, which might hinder the transport of nutrients and metabolites through the hydrogel volume over longer length scales. In this study, fabricated hydrogels were sufficiently small, such that diffusion in any direction from the cell culture media would be <500 μm, thereby avoiding depletion of nutrients or oxygen. Any cell death that occurred could be attributed to apoptosis or other spontaneous cellular mechanisms, and not to hypoxia or necrosis. Likewise, the gradual reduction of mesh size of the PEG-PQ matrix with increasing NVP concentration is expected to have minimal effect on cell viability, apoptosis, proliferation, or metabolic activity, but may hinder the formation of minor cellular protrusions and filopodial sensing of encapsulated cells [42,43]. Notably, the theoretical mesh size estimated in this study range from ~50-70 nm, which is significantly smaller than the size of single cells or individual cellular protrusions. Cells encapsulated in matrices with pore cross sections <7 $\mu m^2$ primarily have to rely on MMP-dependent proteolytic degradation to form invadopodia and invasive clusters [42,44]. Hence, in this hydrogel system, matrix degradability, along with matrix adhesivity, is expected to play a more significant role than mesh size or stiffness in controlling 3D cancer cell behavior, although stiffness cannot be completely ruled out.

Characterization of hydrogel degradation indicates reduced degradability with increased incorporation of non-degradable NVP. It is expected that cells encapsulated in matrices with higher NVP may be limited in degradation of their immediate local matrix, thereby affecting cellular processes including proliferation, invasion and cluster formation. In future studies, the change in expression profile of cancercell secreted MMPs in these different hydrogel matrices could be further investigated to gain insight into matrix permissiveness toward cancer cells. Additionally, investigation of the expression profile of cancer cell-secreted ECM proteins and integrin engagement would shed light on differences in matrix remodeling between dormant and invasive sub-populations.

Investigation of the dormancy-proliferation switch and escape from tumor dormancy program is important toward recapitulation of metastatic relapse. To specifically investigate the role of matrix biochemical properties toward escape from dormancy, we altered matrix adhesivity without influencing matrix crosslink density to induce the phenotypic switch. In hydrogels inducing single cell, restricted survival, dormancy, encapsulated cancer cells were maintained in long-term culture (75 days) during which the rate of decrease in viability and viable cell density gradually slowed over the course of the first 30 days. Upon coupling of PEG-RGDS in the matrix on day 40, cells transitioned to the high growth state with increasing proliferation and viable cell density until day 75 when the experiment was

terminated. This phenomenon is simulative of the situation where stromal cells in the dormant niche secrete proteins that dormant cancer cells can bind to and be directed towards metastatic growth. Although we demonstrate the transition of cancer cells from the single cell restricted survival dormancy state to the high growth state, it can be surmised that addition of PEG-RGDS to PEG-PQ matrices belonging to other dormancy states can also be reactivated toward the high growth state. Similarly, including NVP in the hydrogel matrix along with PEG-RGDS could potentially induce the cells to switch from a single cell dormancy state to a balanced dormancy state or a moderate growth state. Among the current ECM-induced dormancy platforms that model metastatic relapse, the dormancy-proliferation switch is achieved via: 1) partial dissociation of cell-restrictive matrix to increase matrix permissiveness and allow invasive growth [20], 2) complete dissociation of matrix and reseeding of dormant cell clones on two dimensional (2D) surfaces to promote cell spreading and growth [20], and 3) addition of pro-inflammatory cytokines and angiogenic growth factors to encapsulated cells to reactivate specific signaling processes mediating cell cycle progression [27,28]. Complete dissociation of the cell-restrictive matrix leads to loss of dimensional context experienced by cancer cells within native microenvironments and reactivation using soluble signaling factors bypasses the physical and biochemical restriction imposed by the encapsulating matrix. Using the demonstrated approach, cells can be continuously maintained under a dynamic 3D microenvironment, thereby maintaining dimensional context throughout long-term culture.

Tumor dormancy has been studied *in vivo* where cancer cells injected in mice can persist as solitary single cells or form small multicellular foci with balanced apoptosis and proliferation in different organs over several days [11,12,36]. *In vitro* studies have also examined the role of ECM properties in regulating tumor cell behavior in the context of tumor cell phenotype and dormancy [37,45]. Physical confinement of cancer cells in non-degradable matrices or matrices with reduced degradability has been exploited to induce dormancy-like behavior in encapsulated cells [18-21]. Similarly, the findings from this study underscore the role of matrix degradability and adhesivity in regulating cancer cell fate toward tumor dormancy. Although the developed *in vitro* model is limited towards specific cell-matrix interactions (integrin ligation with RGDS), it could be expanded further via incorporation of organ-specific proteins or peptide formulations that better recapitulate the composition of specific secondary organs harboring dormant tumor cells [46-49]. Overall, we demonstrate hydrogel-induced direction of MDA-MB-231 cells toward different phenotypic states. Though this cell line represents the metastatic triple negative breast cancer subtype (TNBC), other breast, prostate, and colon cancer cell lines could be used in future to generalize dormancy studies using the hydrogel platform developed here [50]. Particularly, breast cancer (estrogen receptor, ER+ subtype) and prostate cancer cells are known to lie dormant in the bone marrow for long time periods (years to decades) prior to metastatic growth. Intelligent design of this hydrogel platform, along with co-culture with bone marrow stromal cells, could help establish a synthetic, tunable, bone marrow niche-mimetic hydrogel (with matching physical and biochemical cues) for long-term dormancy studies [47,51,52]. Additionally, genomic and proteomic characterization of dormant and invasive subpopulations in different hydrogel formulations could potentially help identify dormancy signatures and provide dormancy-specific drug targets. In the future, this hydrogel platform

could be implemented for high-content phenotypic screening of compound libraries to identify potential candidates to treat dormant cancer cells [53-57]. This method would eventually help segregate between compounds having differential efficacy against invasive, proliferative populations and dormant, quiescent populations.

## 5. Conclusion

Investigation of ECM-induced changes in 3D cancer cell behavior is important in the context of studying metastasis, invasion and dormancy. *In vitro* models that recapitulate a wide range of these behaviors via modulation of matrix properties can facilitate such investigations. In this study, we demonstrated the ability to tune matrix physical and biochemical properties including crosslink density, degradability, and adhesivity. MDA-MB-231 cells encapsulated within hydrogels with well-controlled properties underwent distinct phenotypic changes as quantified through multiple cellular metrics. Based on these metrics, hydrogel formulations were phenotypically classified into specific states that recapitulated the full spectrum of potential fates experienced by DTCs in secondary tissue niches post extravasation. Specifically, tuning of matrix crosslink density, degradability and adhesivity resulted in direction of cancer cells toward phenotypic states of high growth, moderate growth, single cell restricted survival dormancy, balanced dormancy. Furthermore, dynamic modulation of matrix adhesivity was employed to investigate the transition of cancer cells from a dormant state to a high growth state, recapitulative of metastatic relapse. Overall, this synthetic and tunable hydrogel-based platform facilitates investigation of tumor dormancy and could potentially aid in discovery and development of dormancy-associated molecular targets and drugs.

## Acknowledgements

This work was supported by funding form the National Institutes of Health/ National Cancer Institute IMAT Program (R21CA214299) and the W. M. Keck Foundation (15A00396). The authors would like to acknowledge Omar Banda for help with chemical structures in Fig. 1, Dr. Shuang Liu (Xinqiao Jia research group) for help with GPC analysis and Babak Naghizadehsafa (Dawn Elliott research group) for help with mechanical testing. Confocal microscopy was provided by the Bio-Imaging Center in the Delaware Biotechnology Institute, supported with grants from the NIH-NIGMS (P20 GM103446), the NSF (IIA-1301765) and the State of Delaware.

## References

[1]. Arneson TJ, Shuling Li, Peng Yi, Weinhandl ED, Blaes A, Cetin K, Chia VM, Stryker S, Pinzone JJ, Acquavella J, Estimated number of prevalent cases of metastatic bone disease in the US adult population, Clin. Epidemiol (2012) 87. doi:10.2147/CLEP.S28339. [PubMed: 22570568]

[2]. Chen M-T, Sun H-F, Zhao Y, Fu W-Y, Yang L-P, Gao S-P, Li L-D, Jiang H, Jin W, Comparison of patterns and prognosis among distant metastatic breast cancer patients by age groups: a SEER population-based analysis, Sci. Rep 7 (2017). doi:10.1038/s41598-017-10166-8.

[3]. Mariotto AB, Etzioni R, Hurlbert M, Penberthy L, Mayer M, Estimation of the Number of Women Living with Metastatic Breast Cancer in the United States, Cancer Epidemiol. Prev. Biomark. (2017). doi:10.1158/1055-9965.EPI-16-0889.

[4]. Pradhan S, Sperduto JL, Farino CJ, Slater JH, Engineered in vitro models of tumor dormancy and reactivation, J. Biol. Eng 12 (2018). doi:10.1186/s13036-018-0120-9.

[5]. Gomis RR, Gawrzak S, Tumor cell dormancy, Mol. Oncol 11 (2017) 62–78. doi:10.1016/j.molonc.2016.09.009. [PubMed: 28017284]

[6]. Uhr JW, Pantel K, Controversies in clinical cancer dormancy, Proc. Natl. Acad. Sci. 108 (2011) 12396–12400. doi:10.1073/pnas.1106613108. [PubMed: 21746894]

[7]. Aguirre-Ghiso JA, Models, mechanisms and clinical evidence for cancer dormancy, Nat. Rev. Cancer. 7 (2007) 834–846. doi:10.1038/nrc2256. [PubMed: 17957189]

[8]. Krall JA, Reinhardt F, Mercury OA, Pattabiraman DR, Brooks MW, Dougan M, Lambert AW, Bierie B, Ploegh HL, Dougan SK, Weinberg RA, The systemic response to surgery triggers the outgrowth of distant immune-controlled tumors in mouse models of dormancy, Sci. Transl. Med 10 (2018). doi:10.1126/scitranslmed.aan3464.

[9]. Meng S, Tripathy D, Frenkel EP, Shete S, Naftalis EZ, Huth JF, Beitsch PD, Leitch M, Hoover S, Euhus D, Haley B, Morrison L, Fleming TP, Herlyn D, Terstappen LWMM, Fehm T, Tucker TF, Lane N, Wang J, Uhr JW, Circulating tumor cells in patients with breast cancer dormancy, Clin. Cancer Res 10 (2004) 8152–8162. doi:10.1158/1078-0432.CCR-04-1110. [PubMed: 15623589]

[10]. Grzelak CA, Ghajar CM, Metastasis “systems” biology: how are macro-environmental signals transmitted into microenvironmental cues for disseminated tumor cells?, Curr. Opin. Cell Biol 48 (2017) 79–86. doi:10.1016/j.ceb.2017.06.002. [PubMed: 28715713]

[11]. Luzzi KJ, MacDonald IC, Schmidt EE, Kerkvliet N, Morris VL, Chambers AF, Groom AC, Multistep nature of metastatic inefficiency: dormancy of solitary cells after successful extravasation and limited survival of early micrometastases, Am. J. Pathol 153 (1998) 865–873. doi: 10.1016/S0002-9440(10)65628-3. [PubMed: 9736035]

[12]. Cameron MD, Schmidt EE, Kerkvliet N, Nadkarni KV, Morris VL, Groom AC, Chambers AF, MacDonald IC, Temporal progression of metastasis in lung: cell survival, dormancy, and location dependence of metastatic inefficiency, Cancer Res. 60 (2000) 2541–2546. [PubMed: 10811137]

[13]. Linde N, Fluegen G, Aguirre-Ghiso JA, The relationship between dormant cancer cells and their microenvironment, in: Adv. Cancer Res, Elsevier, 2016: pp. 45–71. doi:10.1016/bs.acr.2016.07.002.

[14]. Bragado P, Sosa MS, Keely P, Condeelis J, Aguirre-Ghiso JA, Microenvironments dictating tumor cell dormancy, in: Ignatiadis M, Sotiriou C, Pantel K (Eds.), Minimal Residual Dis. Circ. Tumor Cells Breast Cancer, Springer Berlin Heidelberg, Berlin, Heidelberg, 2012: pp. 25–39. doi:10.1007/978-3-642-28160-0_3.

[15]. Widner DB, Park SH, Eber MR, Shiozawa Y, Interactions between disseminated tumor cells and bone marrow stromal cells regulate tumor dormancy, Curr. Osteoporos. Rep 16 (2018) 596–602. doi:10.1007/s11914-018-0471-7. [PubMed: 30128835]

[16]. Price TT, Burness ML, Sivan A, Warner MJ, Cheng R, Lee CH, Olivere L, Comatas K, Magnani J, Kim Lyerly H, Cheng Q, McCall CM, Sipkins DA, Dormant breast cancer micrometastases reside in specific bone marrow niches that regulate their transit to and from bone, Sci. Transl. Med 8 (2016) 340ra73. doi:10.1126/scitranslmed.aad4059.

[17]. Rao SS, Kondapaneni RV, Narkhede AA, Bioengineered models to study tumor dormancy, J. Biol. Eng 13 (2019) 3. doi: 10.1186/s13036-018-0137-0. [PubMed: 30647771]

[18]. Pradhan S, Chaudhury CS, Lipke EA, Dual-phase, surface tension-based fabrication method for generation of tumor millibeads, Langmuir. 30 (2014) 3817–3825. doi:10.1021/la500402m. [PubMed: 24617794]

[19]. Preciado JA, Reátegui E, Azarin SM, Lou E, Aksan A, Immobilization platform to induce quiescence in dormancy-capable cancer cells, Technology. 05 (2017) 129–138. doi:10.1142/S2339547817500078.

[20]. Fang JY, Tan S-J, Wu Y-C, Yang Z, Hoang BX, Han B, From competency to dormancy: a 3D model to study cancer cells and drug responsiveness, J. Transl. Med 14 (2016). doi: 10.1186/s12967-016-0798-8.

[21]. Pradhan S, Hassani I, Seeto WJ, Lipke EA, PEG-fibrinogen hydrogels for three-dimensional breast cancer cell culture, J. Biomed. Mater. Res. A. 105 (2017) 236–252. doi:10.1002/jbm.a.35899. [PubMed: 27615742]

[22]. Lampi MC, Reinhart-King CA, Targeting extracellular matrix stiffness to attenuate disease: From molecular mechanisms to clinical trials, Sci. Transl. Med 10 (2018) eaao0475. doi:10.1126/scitranslmed.aao0475. [PubMed: 29298864]

[23]. Aguirre-Ghiso JA, Bragado P, Sosa MS, Targeting dormant cancer, Nat. Med. 19 (2013) 276–277. doi:10.1038/nm.3120. [PubMed: 23467238]

[24]. Hurst RE, Bastian A, Bailey-Downs L, Ihnat MA, Targeting dormant micrometastases: rationale, evidence to date and clinical implications, Ther. Adv. Med. Oncol. 8 (2016) 126–137. doi: 10.1177/1758834015624277. [PubMed: 26929788]

[25]. Barkan D, Kleinman H, Simmons JL, Asmussen H, Kamaraju AK, Hoenorhoff MJ, Liu Z. -y., Costes SV, Cho EH, Lockett S, Khanna C, Chambers AF, Green JE, Inhibition of Metastatic Outgrowth from Single Dormant Tumor Cells by Targeting the Cytoskeleton, Cancer Res. 68 (2008) 6241–6250. doi:10.1158/0008-5472.CAN-07-6849. [PubMed: 18676848]

[26]. Barkan D, El Touny LH, Michalowski AM, Smith JA, Chu I, Davis AS, Webster JD, Hoover S, Simpson RM, Gauldie J, Green JE, Metastatic growth from dormant cells induced by a Col-I-enriched fibrotic environment, Cancer Res. 70 (2010) 5706–5716. doi: 10.1158/0008-5472.CAN-09-2356. [PubMed: 20570886]

[27]. Sosnoski DM, Norgard RJ, Grove CD, Foster SJ, Mastro AM, Dormancy and growth of metastatic breast cancer cells in a bone-like microenvironment, Clin. Exp. Metastasis. 32 (2015) 335–344. doi: 10.1007/s10585-015-9710-9. [PubMed: 25749879]

[28]. Tivari S, Lu H, Dasgupta T, De Lorenzo MS, Wieder R, Reawakening of dormant estrogen-dependent human breast cancer cells by bone marrow stroma secretory senescence, Cell Commun. Signal. 16 (2018). doi:10.1186/s12964-018-0259-5.

[29]. Weber LM, Lopez CG, Anseth KS, Effects of PEG hydrogel crosslinking density on protein diffusion and encapsulated islet survival and function, J. Biomed. Mater. Res. A. 90A (2009) 720–729. doi:10.1002/jbm.a.32134.

[30]. Gill BJ, Gibbons DL, Roudsari LC, Saik JE, Rizvi ZH, Roybal JD, Kurie JM, West JL, A synthetic matrix with independently tunable biochemistry and mechanical properties to study epithelial morphogenesis and EMT in a lung adenocarcinoma model, Cancer Res. (2012) canres. 0895.2012. doi:10.1158/0008-5472.CAN-12-0895.

[31]. Lee C-Y, Teymour F, Camastral H, Tirelli N, Hubbell JA, Elbert DL, Papavasiliou G, Characterization of the network structure of PEG diacrylate hydrogels formed in the presence of N-vinyl pyrrolidone, Macromol. React. Eng 8 (2014) 314–328. doi:10.1002/mren.201300166.

[32]. Turturro MV, Sokic S, Larson JC, Papavasiliou G, Effective tuning of ligand incorporation and mechanical properties in visible light photopolymerized poly(ethylene glycol) diacrylate hydrogels dictates cell adhesion and proliferation, Biomed. Mater 8 (2013) 025001. doi: 10.1088/1748-6041/8/2/025001. [PubMed: 23343533]

[33]. Schweller RM, West JL, Encoding hydrogel mechanics via network cross-linking structure, ACS Biomater. Sci. Eng 1 (2015) 335–344. doi:10.1021/acsbiomaterials.5b00064. [PubMed: 26082943]

[34]. Schweller RM, Wu ZJ, Klitzman B, West JL, Stiffness of protease sensitive and cell adhesive PEG hydrogels promotes neovascularization in vivo, Ann. Biomed. Eng. 45 (2017) 1387–1398. doi:10.1007/s10439-017-1822-8. [PubMed: 28361182]

[35]. Cu Y, Saltzman WM, Mathematical modeling of molecular diffusion through mucus, Adv. Drug Deliv. Rev. 61 (2009) 101–114. doi:10.1016/j.addr.2008.09.006. [PubMed: 19135488]

[36]. Naumov GN, MacDonald IC, Weinmeister PM, Kerkvliet N, Nadkarni KV, Wilson SM, Morris VL, Groom AC, Chambers AF, Persistence of solitary mammary carcinoma cells in a secondary site: a possible contributor to dormancy, Cancer Res. 62 (2002) 2162–2168. [PubMed: 11929839]

[37]. Pradhan S, Smith AM, Garson CJ, Hassani I, Seeto WJ, Pant K, Arnold RD, Prabhakarpandian B, Lipke EA, A microvascularized tumor-mimetic platform for assessing anti-cancer drug efficacy, Sci. Rep 8 (2018). doi:10.1038/s41598-018-21075-9.

[38]. Reynolds DS, Bougher KM, Letendre JH, Fitzgerald SF, Gisladottir UO, Grinstaff MW, Zaman MH, Mechanical confinement via a PEG/Collagen interpenetrating network inhibits behavior characteristic of malignant cells in the triple negative breast cancer cell line MDA.MB.231, Acta Biomater. 77 (2018) 85–95. doi:10.1016/j.actbio.2018.07.032. [PubMed: 30030173]

[39]. Obenauf AC, Massagué J, Surviving at a distance: Organ-specific metastasis, Trends Cancer. 1 (2015) 76–91. doi: 10.1016/j.trecan.2015.07.009.

[40]. Browning MB, Wilems T, Hahn M, Cosgriff-Hernandez E, Compositional control of poly(ethylene glycol) hydrogel modulus independent of mesh size, J. Biomed. Mater. Res. A. 98 (2011) 268–273. doi:10.1002/jbm.a.33109. [PubMed: 21626658]

[41]. Macdougall LJ, Wiley KL, Kloxin AM, Dove AP, Design of synthetic extracellular matrices for probing breast cancer cell growth using robust cyctocompatible nucleophilic thiol-yne addition chemistry, Biomaterials. 178 (2018) 435–447. doi:10.1016/j.biomaterials.2018.04.046. [PubMed: 29773227]

[42]. Caswell PT, Zech T, Actin-based cell protrusion in a 3D matrix, Trends Cell Biol. 28 (2018) 823–834. doi: 10.1016/j.tcb.2018.06.003. [PubMed: 29970282]

[43]. Jacquemet G, Hamidi H, Ivaska J, Filopodia in cell adhesion, 3D migration and cancer cell invasion, Curr. Opin. Cell Biol 36 (2015) 23–31. doi:10.1016/j.ceb.2015.06.007. [PubMed: 26186729]

[44]. Wolf K, te Lindert M, Krause M, Alexander S, te Riet J, Willis AL, Hoffman RM, Figdor CG, Weiss SJ, Friedl P, Physical limits of cell migration: Control by ECM space and nuclear deformation and tuning by proteolysis and traction force, J Cell Biol. 201 (2013) 1069–1084. doi: 10.1083/jcb.201210152. [PubMed: 23798731]

[45]. Pradhan S, Clary JM, Seliktar D, Lipke EA, A three-dimensional spheroidal cancer model based on PEG-fibrinogen hydrogel microspheres, Biomaterials. 115 (2017) 141–154. doi :10.1016/j.biomaterials.2016.10.052. [PubMed: 27889665]

[46]. Brooks EA, Gencoglu MF, Corbett DC, Stevens KR, Peyton S, An omentum-inspired 3D PEG hydrogel for identifying ECM drivers of drug resistant ovarian cancer, bioRxiv. (2019) 560482. doi:10.1101/560482.

[47]. Jansen L, McCarthy T, Lee M, Peyton S, A synthetic, three-dimensional bone marrow hydrogel, (2018). doi: 10.1101/275842.

[48]. Schwartz AD, Barney LE, Jansen LE, Nguyen TV, Hall CL, Meyer AS, Peyton SR, A biomaterial screening approach reveals microenvironmental mechanisms of drug resistance, Integr. Biol 9 (2017) 912–924. doi:10.1039/c7ib00128b.

[49]. Sawicki LA, Ovadia EM, Pradhan L, Cowart JE, Ross KE, Wu CH, Kloxin AM, Tunable synthetic extracellular matrices to investigate breast cancer response to biophysical and biochemical cues, APL Bioeng. 3 (2019) 016101. doi:10.1063/1.5064596. [PubMed: 31069334]

[50]. Kim RS, Avivar-Valderas A, Estrada Y, Bragado P, Sosa MS, Aguirre-Ghiso JA, Segall JE, Dormancy signatures and metastasis in estrogen receptor positive and negative breast cancer, PloS One. 7 (2012) e35569. doi:10.1371/journal.pone.0035569. [PubMed: 22530051]

[51]. Carpenter RA, Kwak J-G, Peyton SR, Lee J, Implantable pre-metastatic niches for the study of the microenvironmental regulation of disseminated human tumour cells, Nat. Biomed. Eng (2018). doi: 10.1038/s41551-018-0307-x.

[52]. LeValley PJ, Kloxin AM, Chemical Approaches to Dynamically Modulate the Properties of Synthetic Matrices, ACS Macro Lett. 8 (2019) 7–16. doi:10.1021/acsmacrolett.8b00808.

[53]. Wenzel C, Riefke B, Gründemann S, Krebs A, Christian S, Prinz F, Osterland M, Golfier S, Räse S, Ansari N, Esner M, Bickle M, Pampaloni F, Mattheyer C, Stelzer EH, Parczyk K, Prechtl S, Steigemann P, 3D high-content screening for the identification of compounds that target cells in dormant tumor spheroid regions, Exp. Cell Res. 323 (2014) 131–143. doi:10.1016/j.yexcr.2014.01.017. [PubMed: 24480576]

[54]. Ramirez M, Rajaram S, Steininger RJ, Osipchuk D, Roth MA, Morinishi LS, Evans L, Ji W, Hsu C-H, Thurley K, Wei S, Zhou A, Koduru PR, Posner BA, Wu LF, Altschuler SJ, Diverse drug-resistance mechanisms can emerge from drug-tolerant cancer persister cells, Nat. Commun 7 (2016) 10690. doi:10.1038/ncomms10690. [PubMed: 26891683]

[55]. Hurst RE, Hauser PJ, You Y, Bailey-Downs LC, Bastian A, Matthews SM, Thorpe J, Earle C, Bourguignon LYW, Ihnat MA, Identification of novel drugs to target dormant micrometastases, BMC Cancer. 15 (2015). doi:10.1186/s12885-015-1409-4.

[56]. Cavnar SP, Rickelmann AD, Meguiar KF, Xiao A, Dosch J, Leung BM, Cai Lesher-Perez S, Chitta S, Luker KE, Takayama S, Luker GD, Modeling selective elimination of quiescent cancer cells from bone marrow, Neoplasia. 17 (2015) 625–633. doi: 10.1016/j.neo.2015.08.001. [PubMed: 26408255]

[57]. Senkowski W, Jarvius M, Rubin J, Lengqvist J, Gustafsson MG, Nygren P, Kultima K, Larsson R, Fryknäs M, Large-Scale gene expression profiling platform for identification of context-dependent drug responses in multicellular tumor spheroids, Cell Chem. Biol 23 (2016) 1428–1438. doi:10.1016/j.chembiol.2016.09.013. [PubMed: 27984028]

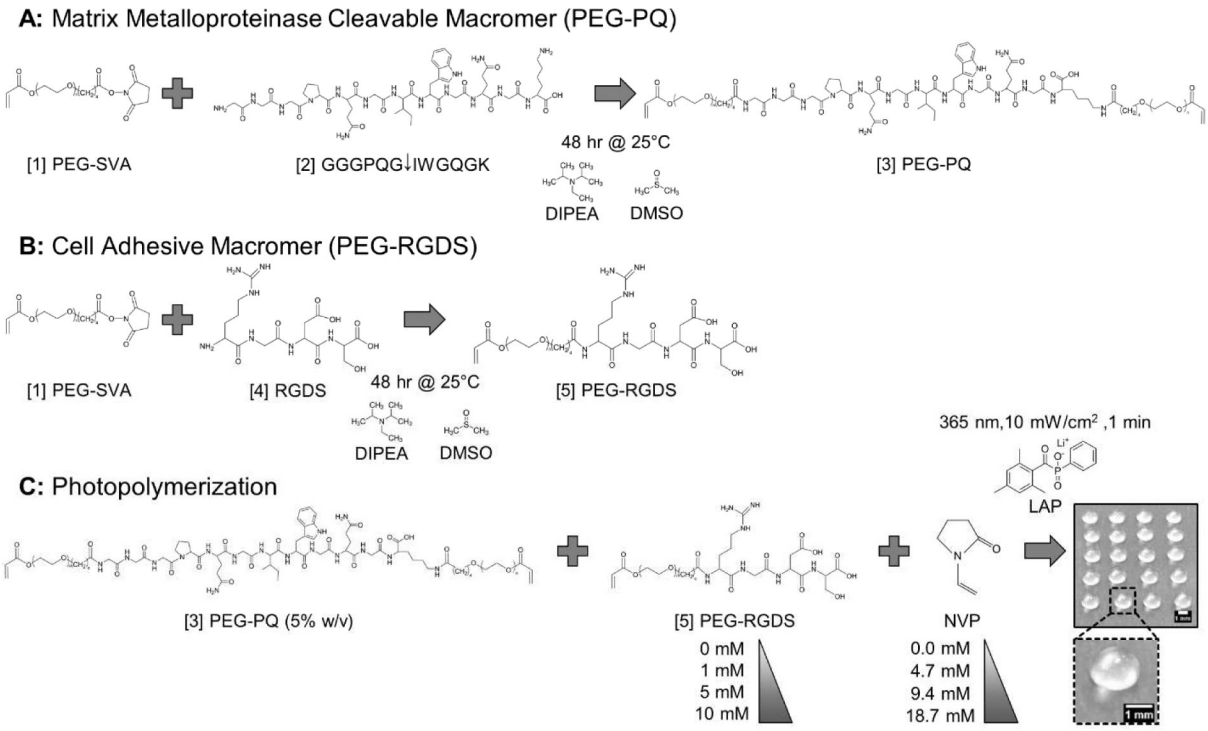


**Fig. 1: Macromer Synthesis & Hydrogel Photopolymerization.**

(A) [1] Acrylate-PEG-SVA (PEG-SVA) was reacted with the matrix metalloproteinase cleavable peptide sequence, [2] GGGPQGIWGQGK (PQ), to yield the [3] PEG-PQ macromer consisting of the PQ sequence flanked by two PEG chains, each containing a terminal acrylate group. (B) A similar reaction was performed with the integrin ligating peptide sequence, [4] RGDS, to yield the [5] PEG-RGDS macromer with one PEG chain with a terminal acrylate group. (C) [3] PEG-PQ (5% w/v) and [5] PEG-RGDS (0-10 mM) were photocrosslinked with the comonomer n-vinyl pyrrolidinone (NVP) (0.0-18.7 mM) via photoinitiation of lithium phenyl-2,4,6-trimethylbenzoyl phosphinate (LAP) to generate 3 μL hydrogel droplets with a diameter of ~1.5 mm and height of ~1 mm (Scale bar = 1 mm). MDA-MB-231 cells were encapsulated at a density of $10\times10^6$ cells/mL and the hydrogels transferred to media containing wells for culture and subsequent analysis.

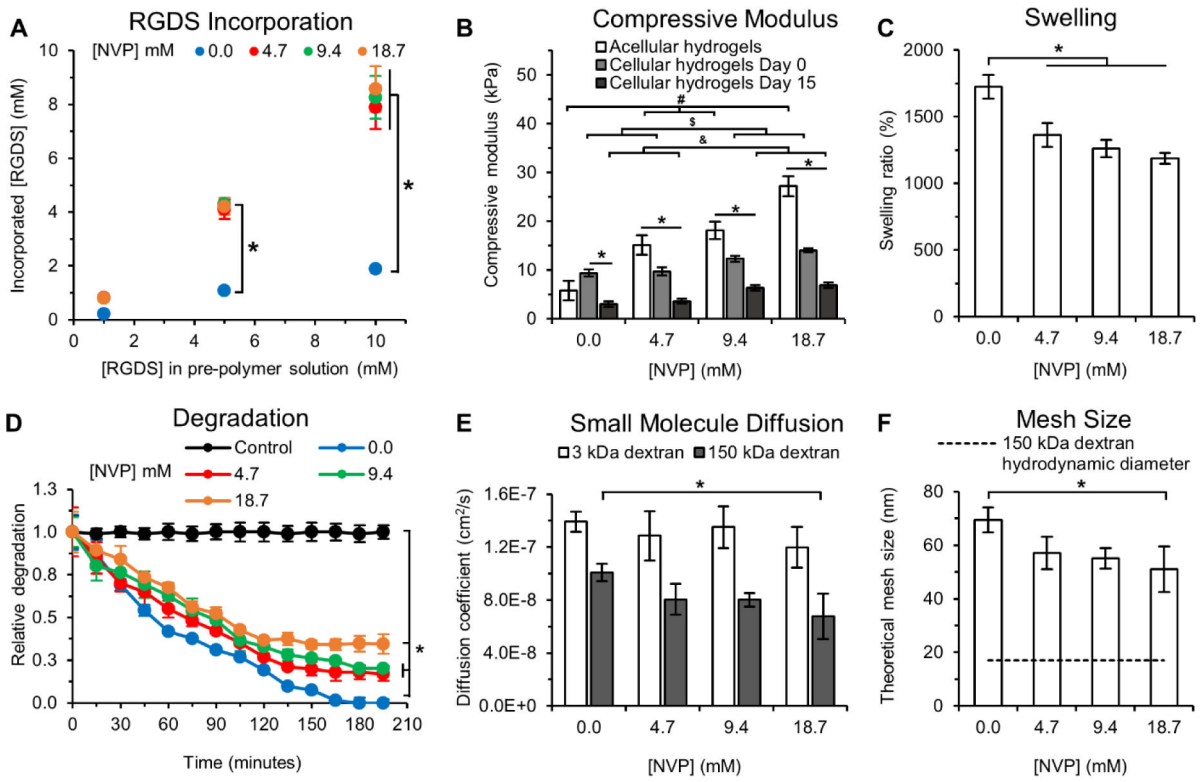


**Fig. 2: Hydrogel Characterization.**

(A) RGDS incorporation into PEG-PQ hydrogels as a function of NVP and PEG-RGDS concentration in the pre-polymer solution. NVP enhanced PEG-RGDS coupling resulting in an incorporation efficiency of 82.3 ± 2.5% which is significantly higher than 20.4 ± 1.1% achieved without NVP. * indicates $p<0.05$. n=4 hydrogels per formulation. (B) Compressive modulus of acellular and cell-laden hydrogels as a function of NVP concentration and cell culture time. Acellular hydrogels with increasing NVP concentration displayed a linear increase in the compressive modulus from 5.8 ± 2.0 kPa to 27.2 ± 2.1 kPa for the 0 and 18.7 mM NVP groups respectively. Day 0, cell-laden hydrogels functionalized with 1 mM RGDS displayed reduced stiffness compared to acellular hydrogels, except for the 0 mM NVP group, and exhibited a moderate linear increase in the compressive modulus with increased NVP concentration from 9.4 ± 0.8 kPa to 14.0 ± 0.4 kPa for the 0 and 18.7 mM NVP groups respectively. By day 15, cell-laden hydrogels were significantly softer than their acellular and day 0 counterparts but still maintained a moderate increase in elastic modulus with increased NVP. #, $, & indicates $p<0.05$ between acellular hydrogels, cellular (day 0) and cellular (day 15) hydrogels respectively; * indicates $p<0.05$ between acellular, cellular (day 0) and cellular (day 15) hydrogels for each NVP concentration. n=3 hydrogels per condition. (C) Hydrogel swelling as a function of NVP concentration. Hydrogels with 4.7-18.7 mM NVP displayed lower swelling compared to those without NVP. * indicates $p<0.05$. n=4 hydrogels per condition. (D) Hydrogel degradation as a function of NVP concentration. NVP incorporation significantly reduced degradability of PEG-PQ hydrogels exposed to collagenase IV in a NVP concentration-dependent manner. The control condition refers to hydrogels with 0 mM NVP incubated in PBS without collagenase to account for

photobleaching. * indicates $p<0.05$. n=4 hydrogels per condition. (E) The effective diffusion coefficient was calculated for 3 kDa and 150 kDa FITC-labeled dextran from release studies. Diffusion of 3 kDa FITC-dextran was not influenced by NVP but diffusion of 150 kDa FITC-dextran was impeded via addition of NVP. (F) The theoretical mesh size of hydrogel networks calculated from release studies of 150 kDa FITC-labeled dextran. A gradual reduction in mesh size with increasing NVP concentration was observed. Dashed line indicates the hydrodynamic diameter of 150 kDa dextran based on the Stokes-Einstein equation. * indicates $p<0.05$. n=4 hydrogels per condition. All values represent mean ± standard deviation.

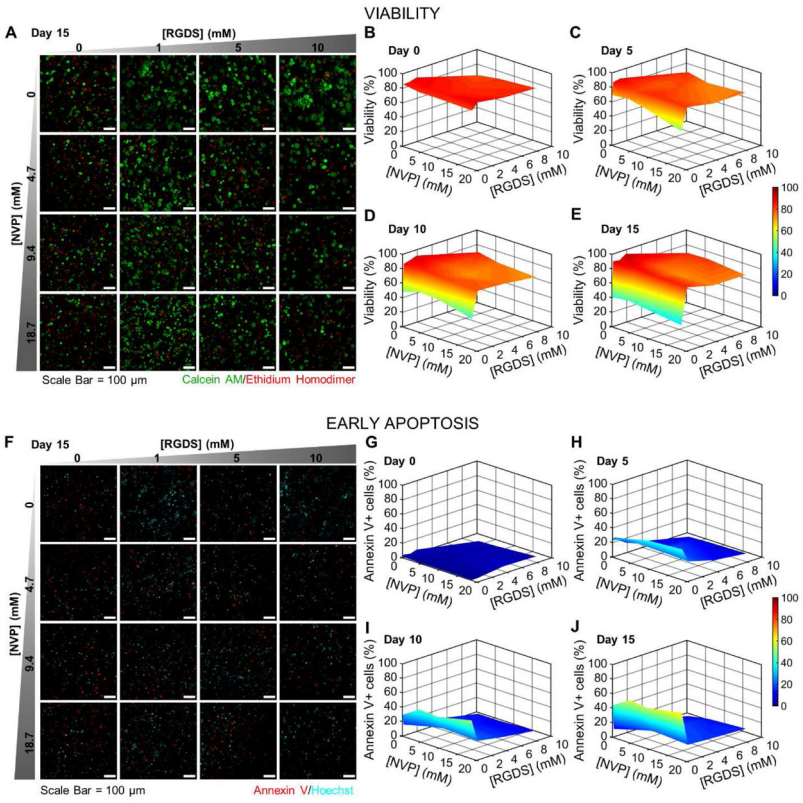


**Fig. 3: Cell Viability & Early Apoptosis.**

(A) Representative maximum intensity z-projections from 3D images stacks of MDA-MB-231s encapsulated in hydrogels with varying NVP and PEG-RGDS concentrations after 15 days in culture. 231s were labeled with calcein AM (green: live cells) and ethidium homodimer (red: dead cells). (B-E) 3D surface plots of cell viability as a function of NVP and PEG-RGDS concentration over 15 days in culture at 5-day intervals. (F) Representative maximum intensity z-projections from 3D image stacks of 231s fluorescently labeled for Annexin V (red: an early apoptosis marker) and Hoechst (cyan: nuclei). (G-J) 3D surface plots of the percent of the cell population positive for Annexin V expression as a function of NVP and PEG-RGDS concentration over 15 days in culture at 5-day intervals. n=6 z-stacks from 3 hydrogels per condition. (A,F) Scale bar = 100 μm.

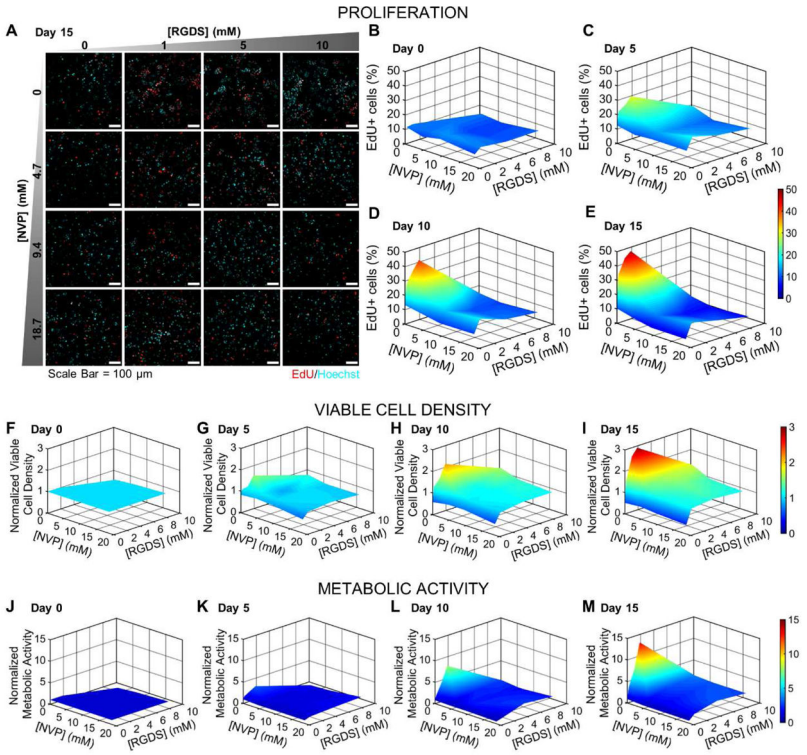


**Fig. 4: Cell Proliferation, Viable Cell Density & Metabolic Activity.**

(A) Representative maximum intensity z-projections from 3D images stacks of MDA-MB-231s encapsulated in hydrogels with varying NVP and PEG-RGDS concentrations after 15 days in culture. Cells were labeled with EdU to indicate active DNA or S-phase synthesis (red) and counterstained with Hoechst (cyan: nuclei). Scale bar = 100 μm. (B-E) 3D surface plots of the percent of the cell population positive for EdU as function of PEG-RGDS and NVP concentration over 15 days in culture at 5-day intervals. (F-I) 3D surface plots of normalized viable cell density as a function of PEG-RGDS and NVP concentration over 15 days in culture at 5-day intervals. All data points were normalized to the initial viable cell density at day 0, 8612 ± 378 cells/mm$^3$ (average ± std. dev. of all hydrogels). n=6 z-stacks from 3 hydrogels per condition. (J-M) 3D surface plots of normalized metabolic activity as a function of PEG-RGDS and NVP concentration over 15 days in culture at 5-day intervals. All data points were normalized to day 0 values for each hydrogel condition. n=5 hydrogels per condition.

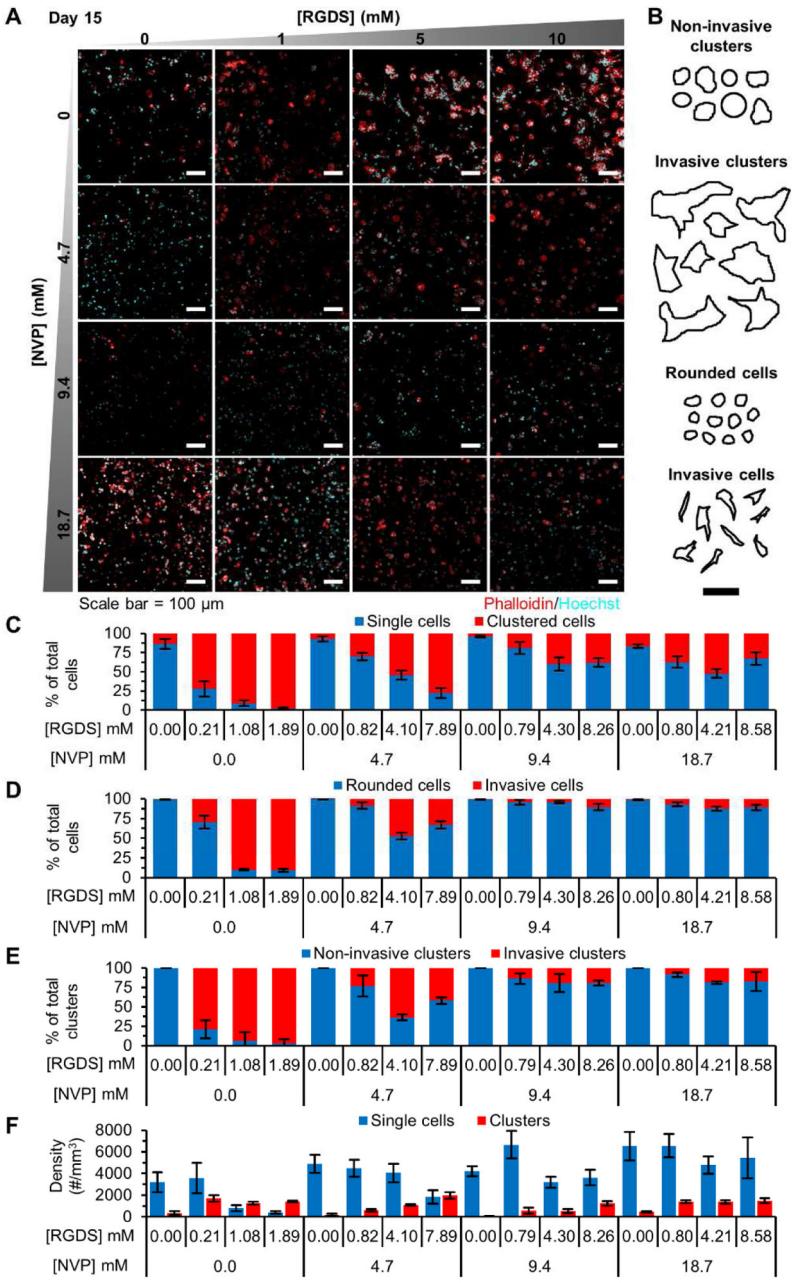


**Fig. 5: Cell & Cell Cluster Morphology Analysis.**

(A) Representative maximum intensity z-projections from 3D image stacks of MDA-MB-231 cells in PEG-PQ hydrogels with varying PEG-RGdS and NVP concentrations fluorescently labeled with phalloidin (red: F-actin) and Hoechst (cyan: nuclei) after 15 days in culture. (B) Representative cell/cluster traces used for classification of cell and cell cluster invasiveness. (A-B) Scale bar = 100 µm. Quantification of (C) the percent of the cell population residing as single cells or in cell clusters, (D) single cell invasiveness based on morphology, (E) cell cluster invasiveness based on morphology, and (F) single cell and cell cluster density in each hydrogel formulation. All data is from day 15 of culture. n=5 z-stacks from 3 hydrogels per condition. All values represent mean ± standard deviation.

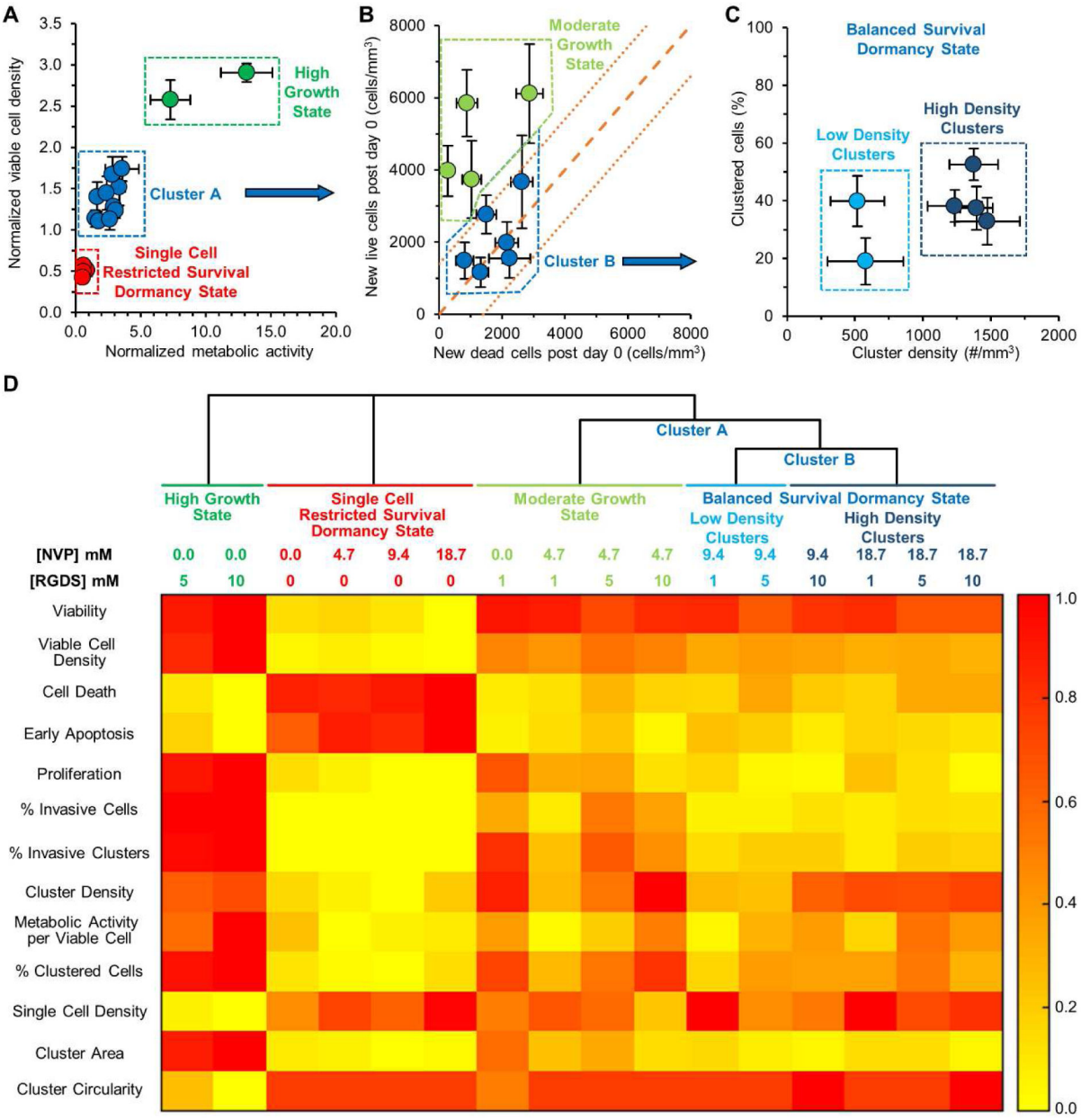


**Fig. 6: Phenotypic Classification of Cancer Cell States.**

The phenotype of MDA-MB-231 cells encapsulated in the 16 different hydrogel formulations was classified via cluster analysis. (A) Plotting normalized viable cell density versus normalized metabolic activity, as measured at day 15, both normalized to day 0 values, revealed three distinct clusters in cell behavior. The uppermost cluster in green contains hydrogels that induced a significant increase in both viable cell density and metabolic activity and were classified as a ‘high growth state’. The lowermost cluster in red contains hydrogels that induced a significant decrease in both viable cell density and metabolic activity and were classified as a ‘single cell, restricted survival, dormant state’. The cluster in blue (Cluster A) was subjected to further analysis. (B) Plotting the appearance of new live cells and new dead cells post encapsulation revealed the potential presence of

two populations of cells, those in a dormant state and those in a moderate growth state. A slope of 1, indicated by the dashed orange line, represents a perfect balance between cell proliferation and death and indicates a situation where the total cell population would not change with time. The smaller dashed orange lines represent error in these measurements. Hydrogels that fell above the error of the line were characterized as a 'moderate growth state' while those falling within the error were characterized as a 'balanced survival, dormancy state'. Those in the dormancy state (Cluster B) were subjected to further analysis. (C) Plotting the percent of clustered cells versus the cluster density indicates that all six hydrogels induced a similar percentage of the cell population to form clusters but with variations in cluster density. Though cells in these hydrogel formulations were in a dormant state, four of the hydrogel formulations (darker blue cluster on the right) induced a significantly higher cell cluster density. (A-C) Each point represents a PEG-PQ hydrogel matrix with a specific PEG-RGDS and NVP concentration. Values represent average ± standard deviation. (D) Heat map of hydrogels categorized into four states based on a phenotype score ranging from 0.0 to 1.0 estimated from specific cellular metrics.

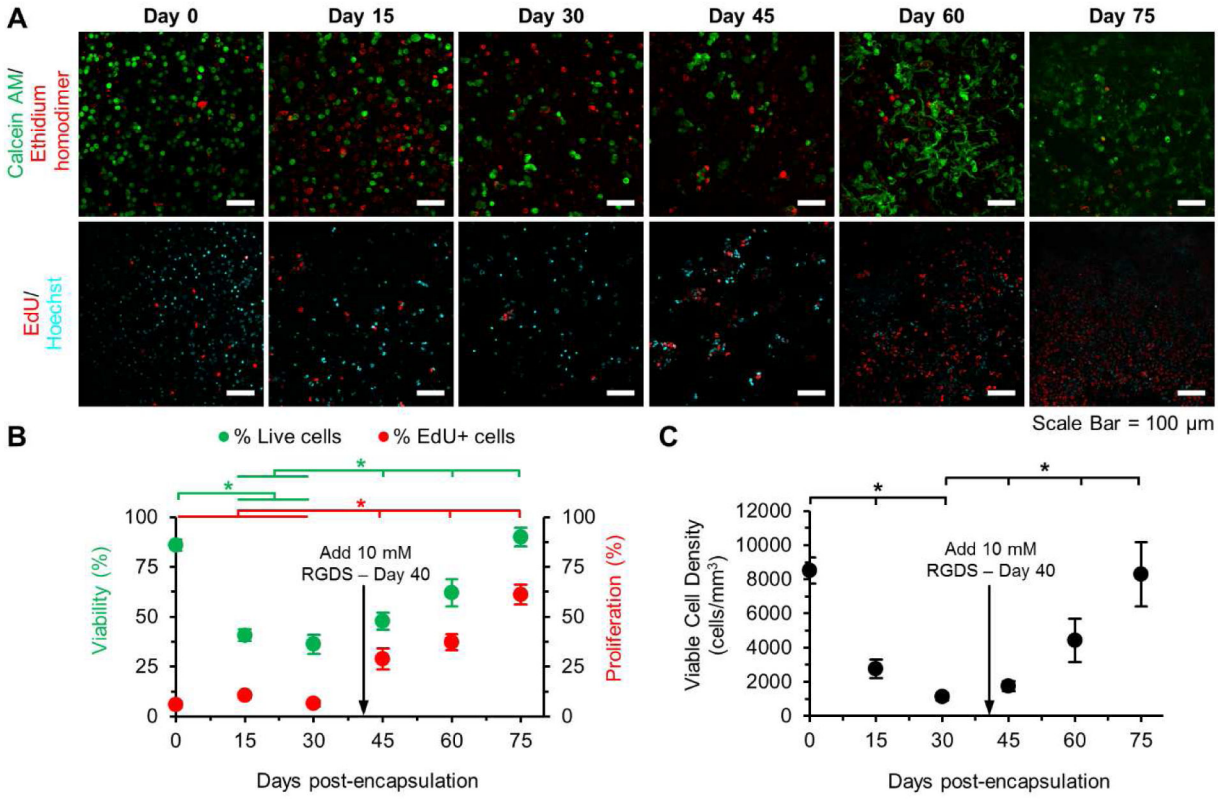


**Fig. 7: Reactivation of Dormant Tumor Cells.**

(A) Representative maximum intensity z-projections from 3D image stacks of MDA-MB-231s encapsulated in hydrogels with 0 mM PEG-RGDS and 0.0 mM NVP on day 0, activated with 10 mM PEG-RGDS on day 40 and cultured for 35 additional days. Top row: cells labeled with calcein AM (green: live cells) and ethidium homodimer (red: dead cells). Bottom row: cells labeled with EdU (red: proliferative cells) and Hoechst (cyan: nuclei). Scale bar = 100 μm. (B) Quantification of cell viability (green), proliferation (red) and (C) viable cell density over 75 days. Arrow indicates coupling of 10 mM PEG-RGDS. * indicates $p<0.05$. n=6 z-stacks from 3 hydrogels per condition. Values represent mean ± standard deviation.

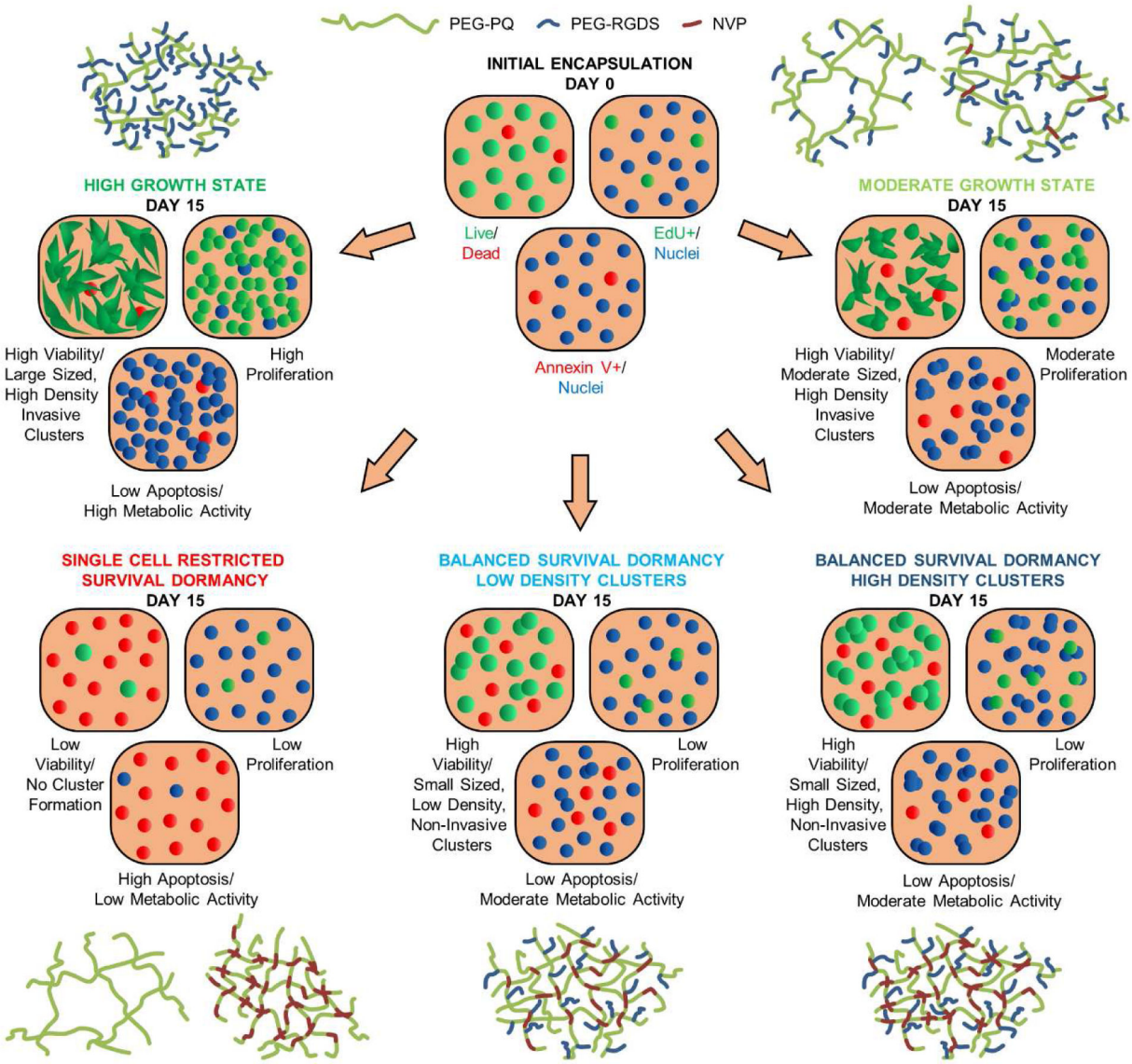


**Fig. 8: Proposed Scheme.**

Based on physical and biochemical properties of the matrix, cancer cells can be directed toward one of four states: 1) high growth, 2) moderate growth, 3) single cell, restricted survival, dormancy, and 4) balanced survival dormancy. When cells are encapsulated within hydrogels with high degradability and high adhesivity, they are directed towards the high growth state. When the matrix degradability is slightly increased, or matrix adhesivity is decreased, they are restricted to a moderate growth state. In the complete absence of matrix adhesivity, cells are induced towards single cell, restricted survival, dormancy. When matrix degradability is further decreased, cells are restricted towards a balanced survival state (with low or high cluster density).